5-7-2005

# THE PREDICTION OF FULLY-DEVELOPED FRICTION FACTORS AND NUSSELT NUMBERS FOR RANDOMLY-ROUGH SURFACES

Spencer Haynes Manning

# THE PREDICTION OF FULLY-DEVELOPED FRICTION FACTORS AND NUSSELT NUMBERS FOR RANDOMLY ROUGH SURFACES

By

Spencer Haynes Manning

A Thesis
Submitted to the Faculty of
Mississippi State University
in Partial Fulfillment of the Requirements
for the Degree of Master of Science
in Mechanical Engineering
in the Department of Mechanical Engineering

Mississippi State, Mississippi

May 2005

THE PREDICTION OF FULLY-DEVELOPED FRICTION FACTORS AND

NUSSLET NUMBERS FOR RANDOMLY-ROUGH SURFACES

By

Spencer Haynes Manning

Approved:

| | |
|---|---|
| B. Keith Hodge<br>Professor of Mechanical Engineering<br>(Director of Thesis) | W. Glenn Steele<br>Professor and Head of Mechanical Engineering<br>(Committee Member) |
| Louay M. Chamra<br>Associate Professor of Mechanical Engineering<br>(Committee Member) | Rogelio Luck<br>Associate Professor of Mechanical Engineering and Director of Graduate Studies in Mechanical Engineering |

W. Glenn Steele
Interim Dean of the College of Engineering

Name: Spencer Haynes Manning

Date of Degree: May 7, 2005

Institution: Mississippi State University

Major Field: Mechanical Engineering

Major Professor: Dr. B. Keith Hodge

Title of Study: THE PREDICTION OF FULLY-DEVELOPED FRICTION FACTORS AND NUSSELT NUMBERS FOR RANDOMLY-ROUGH SURFACES

Pages in Study: 53

Candidate for Degree of Master of Science

A computer program based on the discrete-element method has been developed to compute friction factors and Nusselt Numbers for fully-developed turbulent flows with randomly-rough surfaces. Formulations of the discrete-element model for fully-developed turbulent flows inside circular pipes and between infinite parallel plates with the necessary adaptations for randomly-rough surfaces are provided. Utilizing the output of a three-dimensional profilometer, proper description of the randomly-rough surface is necessary for use within the discrete-element model. Proper description of the randomly-rough surface is achieved by the McClain (2002) method of characterization.

Predictions from the discrete-element model computer program are compared with the classical, laminar and turbulent, smooth-wall results. In addition to the smooth-wall evaluations, predictions are compared with experimental results for turbulent internal flows with deterministic surface roughness. Predictions from the model demonstrated excellent agreement in all cases. Friction factor and Nusselt Number

predictions for fully-developed flows over randomly-rough surfaces are also presented. With the friction factor and Nusselt Number data, velocity profiles for flows over randomly-rough, deterministically-rough and smooth surfaces are provided for comparison.

ACKNOWLEDGEMENTS

I would like to convey my deepest thanks to my family for their continued support in all of my endeavors. They deserve more thanks than I can ever give. To Dr. B. K. Hodge, thank you for your guidance, advice and willingness to explain throughout this undertaking. To the other members of my committee: Dr. Glenn Steele and Dr. Louay Chamra, thank you for your advice and willingness to listen. Also, to Dr. Stephen McClain at the University of Alabama – Birmingham, thank you for your help in making this work possible.

TABLE OF CONTENTS

APPENDIX

LIST OF TABLES

LIST OF FIGURES

FIGURE Page

NOMENCLATURE

| | |
|---|---|
| $A_c$ | Cross-sectional area |
| $A_p$ | Projected area |
| $A_s$ | Surface area |
| $C_D$ | Drag coefficient |
| $c_p$ | Specific heat |
| $D_h$ | Hydraulic diameter |
| d | Local element diameter |
| $F_D$ | Drag force |
| $f_f$ | Fanning friction factor |
| h | Half plate spacing |
| $\bar{h}$ | Heat transfer coefficient |
| K | Thermal conductivity |
| $K_T$ | Turbulent thermal conductivity |
| L | Streamwise element spacing |
| L* | Eddy viscosity parameter |
| L** | Eddy conductivity parameter |
| $l$ | Transverse element spacing |
| $\ell_m$ | Mixing length |
| Nu | Nusselt number |
| $Nu_d$ | Local element Nusselt number |

| | |
|---|---|
| P | Pressure |
| Pr | Prandtl number |
| $Pr_T$ | Turbulent Prandtl number |
| $\dot{Q}$ | Heat transfer rate |
| $\dot{q}$ | Heat flux |
| R | Radius of circular pipe |
| r | Radius |
| Re | Reynolds number |
| $Re_d$ | Local element Reynolds number |
| T | Temperature |
| $T_m$ | Mixing-cup temperature |
| $T_0$ | Wall temperature |
| $U_m$ | Mean velocity |
| u | Local streamwise velocity |
| x | Streamwise coordinate |
| y | Coordinate normal to wall |

Greek

| | |
|---|---|
| $\alpha$ | Thermal diffusivity |
| $\beta$ | Openage factor |
| $\delta x$ | x-length of control volume |
| $\delta y$ | y-length of control volume |
| $\varepsilon$ | Elliptical eccentricity factor |

| | |
|---|---|
| $\theta$ | Nondimensional temperature |
| $\mu$ | Dynamic viscosity |
| $\mu_T$ | Turbulent eddy viscosity |
| $\rho$ | Density |

Superscripts

| | |
|---|---|
| $\sim$ | Indicates nondimensionalization = $\cdot / R$ (circular pipe) or $\cdot / h$ (infinite parallel plates), except $\tilde{u} = u / U_m$ and $\tilde{\theta} = \theta / Nu$. |

# CHAPTER I

# INTRODUCTION

Roughness effects are an important concern on many surfaces of engineering interest. Examples include turbines, compressors, heat exchangers, ships, submarines, aircraft, re-entry vehicles, and piping networks. In these applications, turbulent flows over rough surfaces result in appreciably larger skin friction and heat transfer as compared with corresponding turbulent flows over smooth surfaces. Dependant on the particular application, the increase in skin friction and heat transfer due to the surface roughness can have a beneficial or detrimental effect. Gas turbine performance is negatively affected by the presence of surface roughness. The increased drag on the turbine blades, from the presence of surface roughness, reduces the overall efficiency of the gas turbine. However, for internal cooling of electrical components, increased heat transfer from the presence of surface roughness is desirable. Therefore, the ability to quantify the characteristics of such roughness is necessary.

## Background

Over the years, two methods have emerged for assessing the effects of surface roughness on drag and heat transfer. The first, the equivalent sand-grain roughness model, was proposed by Schlichting (1936). This entirely empirical model compares a rough surface of interest to data from Nikuradse (1933) for flow in pipes roughened by varying sizes of sand. The rough surface of interest is then assigned an equivalent sand-

grain roughness height corresponding to the sand-grain size used in Nikuradse's experiment.

In the same paper that Schlichting introduced the equivalent sand-grain roughness concept, he discussed the significance of the roughness density on the flow resistance. He suggested that the flow resistance of a rough surface could be divided into two components: 1) that due to the sum of the drag from each individual roughness element protruding into the boundary layer and 2) that due to the viscous shear on the smooth part of the wall between the roughness elements. Based on Schlicting's proposal, Taylor (1983) derived and validated the discrete-element model for three-dimensional, ordered roughness elements on a flat plate. Using the output from a three-dimensional profilometer, McClain (2002) presented and validated a method for determining the geometry input required in the discrete-element method for randomly-rough surfaces.

**Objective**

The objective of this work is to develop a computer program for predicting the friction factor and heat transfer for fully-developed flows over randomly-rough surfaces utilizing the discrete-element model. Initially, the discrete-element model is formulated for fully-developed flows in a circular pipe and between parallel plates. The adaptations to the discrete-element for randomly-rough surface considerations are then presented. The randomly-rough surface adaptations presented were developed by McClain (2002). Finally, validation cases and comparisons of the results are presented.

# CHAPTER II

# DISCRETE ELEMENT FORMULATION FOR FULLY-DEVELOPED FLOWS

The discrete-element model as derived by Taylor (1983) is the roughness model used herein. In contrast to the entirely empirical equivalent sand-grain roughness model, the discrete-element model considers the physical characteristics of the roughness elements in the formulation of the differential equations. The roughness effects are integrated into the solution by considering the flow blockage due to the roughness elements, the drag force exerted on the flow by the roughness elements, and the heat transfer between the flow and the roughness elements. The differential equations, with roughness effects, are formulated by applying the basic statements of mass, momentum, and energy conservation to a differential control volume such as that shown in Figure 2.1.

## Circular Pipe Formulation

For the flow blockage, an openage factor, $\beta$, must be defined. Let $\beta_x$ $(\beta_y)$ be the fraction of the surface open to the flow that is perpendicular to the x-coordinate (y-coordinate). The drag force is a result of the roughness elements penetrating the control volume. In terms of a local drag coefficient, the drag force is expressed as

$$F_D = \frac{1}{2}\rho C_D u^2 A_p N_{elements} \tag{2.1}$$

where proper formulation of the discrete-element model requires roughness elements for which the element cross section can be defined at every height, y. Initially,

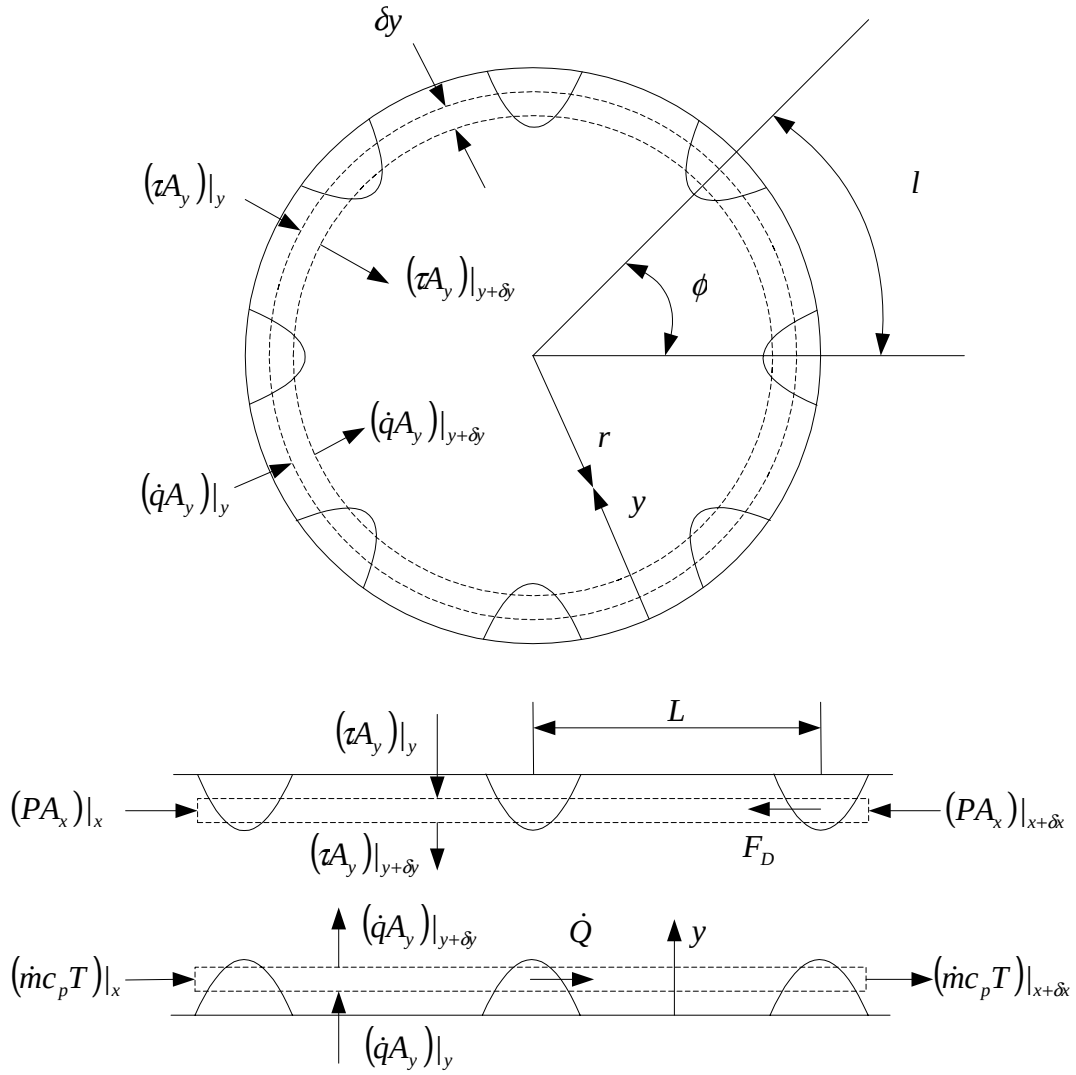


Figure 2.1 Circular Pipe Control Volume.

the roughness elements will be taken to have circular cross-sections with a projected area of $A_p = d(y)\delta y$. The number of elements in the control volume is

$$N_{elements} = \frac{(2\pi R \delta x)}{lL} \tag{2.2}$$

The difference in temperature between the surface of the roughness element penetrating the control volume and the fluid results in the local heat transfer rate, $\dot{Q}$. Using a local Nusselt number, the local heat transfer rate is defined as

$$\dot{Q} = \frac{K}{d(y)} Nu_d A_s N_{elements} (T_0 - T) \tag{2.3}$$

The temperature of the roughness element is taken to be equal to the wall temperature, $T_0$. The local surface area is $A_s = \pi d(y)\delta y$.

In this formulation, the flow is considered to be fully developed, incompressible, and to have constant fluid properties. Considering the aforementioned principles, Taylor and Hodge (1993) presented the steady, fully-developed, Reynolds averaged, two-dimensional turbulent momentum and energy equations with uniform roughness as

$$0 = \frac{\mu}{r}\frac{d}{dy}\left[r\beta_y\left(1+\frac{\mu_T}{\mu}\right)\frac{\partial u}{\partial y}\right] - \beta_x \frac{dP}{dx} - \frac{1}{2}\rho C_D u^2 \frac{d(y)R}{rlL} \tag{2.4}$$

and

$$0 = \rho c_p \beta_x u r \frac{\partial T}{\partial x} - K\frac{\partial}{\partial y}\left[r\beta_y\left(1+\frac{K_T}{K}\right)\frac{\partial T}{\partial y}\right] - KNu_d \frac{\pi R}{lL}(T_0 - T) \tag{2.5}$$

The boundary conditions for equations (2.4) and (2.5) are

$$y = 0 : u = 0,\ T = T_0 \tag{2.6}$$

$$y = R : \frac{du}{dy} = 0,\ \frac{\partial T}{\partial y} = 0$$

The first boundary condition is applied at the pipe wall or y = 0. At this point, the "no-slip" condition is applied and the temperature of the fluid directly adjacent to the surface is taken to be equal to the surface temperature. At the centerline of the pipe, the second boundary condition represents the symmetrical characteristic of the control volume.

Hydrodynamic fully-developed flows are characterized by the relationship, $\partial u / \partial x = 0$. However, the existence of the thermally-developed flow is not as easily visualized. Use of the condition $\partial T / \partial x = 0$ leads only to the adiabatic condition. To properly portray a generalized temperature profile that is independent of the tube length, the variable, $T_m$, must be defined. The mass-averaged fluid temperature or mixing-cup temperature, $T_m$, characterizes the average thermal energy state of the fluid. This temperature is defined as

$$T_m = \frac{1}{UA_c} \int uTdA_c \tag{2.7}$$

While considering the mass-averaged fluid temperature in the definition of the heat flux at the surface under consideration Kays and Crawford (1993) showed that the heat transfer coefficient, $\bar{h}$, for thermally-developed flow is not a function of tube length.

The nondimensional temperature used to characterize thermally-developed flows is defined as

$$\theta = \frac{T_0(x) - T(x,r)}{T_0(x) - T_m(x)} \tag{2.8}$$

For thermally-developed flow, $\theta$ is not a function of the streamwise coordinate x; that is, $\partial \theta / \partial x = 0$. The relationships $\bar{h}$ = constant and $\partial \theta / \partial x = 0$, used to define thermally-developed flow, have been held as true for smooth wall flows. Taylor and Hodge (1992) demonstrated that these relationships held in roughness dominated flows as well.

Two surface conditions commonly specified for the energy equation are for constant wall heat flux and for constant wall temperature. Employing these boundary conditions and the thermally-developed flow relationships, greatly simplify the energy equations. For pipe flow, the Nusselt number is defined as

$$Nu = \frac{2R\dot{q}_0}{K(T_0 - T_m)} = \frac{2R\bar{h}}{K} \tag{2.9}$$

For constant wall heat flux and thermally-developed flow, the following relationships can be established

$$\frac{\partial T}{\partial x} = \frac{\partial T_0}{\partial x} = \frac{\partial T_m}{\partial x} = \frac{\alpha}{U_m R^2} Nu(T_0 - T_m) \tag{2.10}$$

Substituting into equation (2.5) and using the nondimensional variables $\tilde{u} = u/U_m$, $\tilde{y} = y/R$, $\tilde{r} = r/R = 1 - \tilde{y}$, $\tilde{l} = l/R$, and $\tilde{L} = L/R$ and rearranging gives the differential equation for constant wall heat flux.

$$\beta_x \tilde{u} Nu = -\frac{1}{\tilde{r}} \frac{d}{d\tilde{y}} \left[ \tilde{r} \beta_y \left( 1 + \frac{K_T}{K} \right) \frac{d\theta}{d\tilde{y}} \right] + \frac{1}{\tilde{r}} Nu_d \frac{\pi\theta}{\tilde{l}\tilde{L}} \tag{2.11}$$

For constant $T_0$ and thermally-developed flow, the following relationship can be established

$$\frac{\partial T}{\partial x} = \theta \frac{\partial T_m}{\partial x} = \theta \frac{\alpha}{U_m R^2} Nu(T_0 - T_m) \tag{2.12}$$

The energy equation for constant wall temperature then reduces to

$$\beta_x \tilde{u} \theta Nu = -\frac{1}{\tilde{r}} \frac{d}{d\tilde{y}} \left[ \tilde{r} \beta_y \left( 1 + \frac{K_T}{K} \right) \frac{d\theta}{d\tilde{y}} \right] + \frac{1}{\tilde{r}} Nu_d \frac{\pi\theta}{\tilde{l}\tilde{L}} \tag{2.13}$$

The boundary conditions for both equation (2.11) and equation (2.13) are

$$\tilde{y} = 0: \ \theta = 0 \tag{2.14}$$

$$\tilde{y} = 1: \ \frac{d\theta}{d\tilde{y}} = 0$$

**Infinite Parallel Plates Formulation**

The above formulation will now be adapted to consider flows between infinite parallel plates. Figure 2.2 displays the modified differential control volume for the application of the basic conservation statements. Correctly identifying the hydraulic diameter, $D_h$ is essential in considering flows between infinite parallel plates. The hydraulic diameter is defined as

$$D_h = \frac{4A_c}{P} \tag{2.15}$$

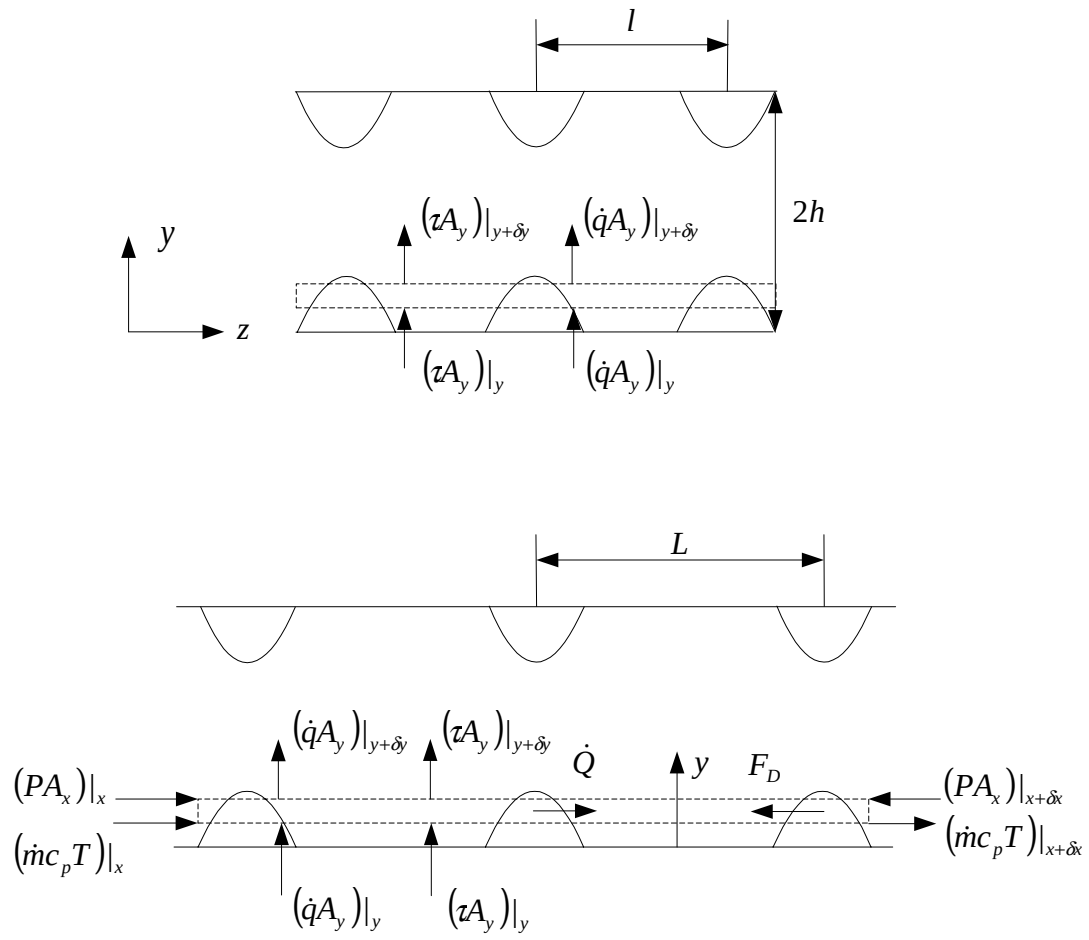


Figure 2.2 Infinite Parallel Plates Control Volume.

For flows between infinite parallel plates, the hydraulic diameter becomes twice the plate spacing or 4h.

For infinite parallel plates, the Reynolds number and Nusselt number based on hydraulic diameter become

$$\mathrm{Re}_{D_h} = \frac{\rho U_m D_h}{\mu} = \frac{\rho U_m 4h}{\mu} \tag{2.16}$$

and

$$Nu = \frac{D_h \bar{h}}{K} = \frac{4h\bar{h}}{K} \tag{2.17}$$

respectively.

The steady, Reynolds averaged, two-dimensional turbulent momentum and energy equations with uniform roughness for fully-developed, incompressible flows between infinite parallel plates with constant fluid properties are

$$0 = \mu \frac{d}{dy}\left[\beta_y \left(1 + \frac{\mu_T}{\mu}\right)\frac{\partial u}{\partial y}\right] - \beta_x \frac{dP}{dx} - \frac{1}{2}\rho C_D u^2 \frac{d(y)}{lL} \tag{2.18}$$

and

$$0 = \rho c_p \beta_x u \frac{\partial T}{\partial x} - K\frac{\partial}{\partial y}\left[\beta_y \left(1 + \frac{K_T}{K}\right)\frac{\partial T}{\partial y}\right] - KNu_d \frac{\pi}{lL}(T_0 - T) \tag{2.19}$$

The boundary conditions for equations (2.18) and (2.19) are

$$y = 0 : u = 0,\ T = T_0 \tag{2.20}$$

$$y = h : \frac{du}{dy} = 0,\ \frac{\partial T}{\partial y} = 0$$

The constant wall heat flux and constant wall temperature boundary conditions previously considered in circular pipe flows will be implemented in the infinite parallel plate formulation as well. Using these common boundary conditions and the thermally-

developed flow relationships in conjunction with the Nusselt number allows for similar simplifications of the energy equations. After applying the constant wall heat flux boundary condition and using the new nondimensional variables $\tilde{y} = y/h$, $\tilde{l} = l/h$, and $\tilde{L} = L/h$, the energy equation reduces to

$$\beta_x \tilde{u} Nu = -4 \frac{d}{d\tilde{y}} \left[ \beta_y \left( 1 + \frac{K_T}{K} \right) \frac{d\theta}{d\tilde{y}} \right] + 4 Nu_d \frac{\pi\theta}{\tilde{l}\tilde{L}} \tag{2.21}$$

The length variables for the infinite parallel plate formulation are nondimensionalized by h, half the plate spacing. The energy equation with the constant wall temperature boundary condition reduces to

$$\beta_x \tilde{u} \theta Nu = -4 \frac{d}{d\tilde{y}} \left[ \beta_y \left( 1 + \frac{K_T}{K} \right) \frac{d\theta}{d\tilde{y}} \right] + 4 Nu_d \frac{\pi\theta}{\tilde{l}\tilde{L}} \tag{2.22}$$

The boundary conditions for both equation (2.21) and equation (2.22) are

$$\tilde{y} = 0 : \ \theta = 0 \tag{2.23}$$

$$\tilde{y} = 1 : \ \frac{d\theta}{d\tilde{y}} = 0$$

**Solution Procedure**

Due to the assumption of constant property, incompressible flow, the momentum and energy equations can be solved separately. However, the velocity profile from the momentum equation solution is required in the solution of the energy equation. The following explanation of the solution method includes equations for both the circular pipe and infinite parallel plate formulations. When the equations differ between the two formulations, an a or b in the equation number will represent the appropriate equation for flows in a circular pipe or between infinite parallel plates, respectively.

Initially, the pressure drop is defined in terms of the Fanning friction factor, $f_f$.

$$\frac{dP}{dx} = -\rho f_f \frac{U_m^{\,2}}{R} \tag{2.24a}$$

$$\frac{dP}{dx} = -\rho f_f \frac{U_m^{\,2}}{2h} \tag{2.24b}$$

The eddy viscosity parameter, L*, is defined such that

$$L^* = \tilde{r}\beta_y\left(1+\frac{\mu_T}{\mu}\right) \tag{2.25a}$$

$$L^* = \beta_y\left(1+\frac{\mu_T}{\mu}\right) \tag{2.25b}$$

Substituting into the momentum equation, reducing, and using the prime notation to represent differentiation with respect to $\tilde{y}$ gives

$$\tilde{u}'' + \frac{L^{*\prime}}{L^*}\tilde{u}' - \left(\frac{1}{4L^*}\mathrm{Re}_D\frac{\tilde{d}}{\tilde{l}\tilde{L}}C_D\tilde{u}\right)\tilde{u} + \frac{1}{2L^*}\beta_x\,\mathrm{Re}_D\,f_f\left(1-\tilde{y}\right) = 0 \tag{2.26a}$$

$$\tilde{u}'' + \frac{L^{*\prime}}{L^*}\tilde{u}' - \left(\frac{1}{8L^*}\mathrm{Re}_{D_h}\frac{\tilde{d}}{\tilde{l}\tilde{L}}C_D\tilde{u}\right)\tilde{u} + \frac{1}{8L^*}\beta_x\,\mathrm{Re}_{D_h}\,f_f = 0 \tag{2.26b}$$

The boundary conditions are

$$\tilde{y} = 0:\ u = 0 \tag{2.27}$$

$$\tilde{y} = 1:\ \tilde{u}' = 0$$

Scaggs et al. (1988) presented the following equation for determination of the blockage factors

$$\beta_y = \beta_x = 1 - \frac{\pi\tilde{d}^{\,2}}{4\tilde{l}\tilde{L}\left(1-\tilde{y}\right)} \tag{2.28a}$$

$$\beta_y = \beta_x = 1 - \frac{\pi \tilde{d}^2}{4 \tilde{l} \tilde{L}} \tag{2.28b}$$

The element diameter, d, is nondimensionalized by R for the circular pipe formulation and h for the infinite parallel plate formulation. The nondimensional element diameter, $\tilde{d}$, is then determined as a function of the element base diameter and height.

A two-band algebraic model, taken from Kays and Crawford (1993), is used for the eddy viscosity. A Prandtl mixing-length model with van Driest damping is used in the viscous sublayer near the wall

$$\frac{\mu_T}{\mu} = \frac{1}{2} \mathrm{Re}_D \, \tilde{\ell}_m^2 \left| \frac{\partial \tilde{u}}{\partial \tilde{y}} \right| \tag{2.29a}$$

$$\frac{\mu_T}{\mu} = \frac{1}{4} \mathrm{Re}_{D_h} \, \tilde{\ell}_m^2 \left| \frac{\partial \tilde{u}}{\partial \tilde{y}} \right| \tag{2.29b}$$

where the nondimensional mixing length, $\tilde{\ell}_m$, is

$$\tilde{\ell}_m = 0.4 \tilde{y} \left[ 1 - \exp\left( \frac{-\frac{1}{2} \mathrm{Re}_D \sqrt{\frac{f_f}{2}} \tilde{y}}{26} \right) \right] \tag{2.30a}$$

$$\tilde{\ell}_m = 0.4 \tilde{y} \left[ 1 - \exp\left( \frac{-\frac{1}{4} \mathrm{Re}_{D_h} \sqrt{\frac{f_f}{2}} \tilde{y}}{26} \right) \right] \tag{2.30b}$$

In the turbulent core of the flow, the relationship becomes

$$\frac{\mu_T}{\mu} = 0.4 \frac{1}{2} \mathrm{Re}_D \frac{\sqrt{f_f / 2}}{6} \tag{2.31a}$$

$$\frac{\mu_T}{\mu} = 0.4\frac{1}{2}\mathrm{Re}_{D_h}\frac{\sqrt{f_f/2}}{12} \tag{2.31b}$$

The limit between the domains of equations (2.28) and (2.30) is taken to be the point where they give the same value for the eddy viscosity relationship, $\mu_T / \mu$.

The functional form of the local element drag coefficient comes from Taylor et al. (1984). This equation is expressed in terms of the local element Reynolds number, $\mathrm{Re}_d$, as

$$C_D = \left(\frac{\mathrm{Re}_d}{1000}\right)^{-0.125}; \quad C_D \succ 0.6 \tag{2.32}$$

$$C_D = 0.6; \quad \text{otherwise}$$

where

$$\mathrm{Re}_d = \frac{1}{2}\mathrm{Re}_D\,\tilde{d}\tilde{u} \tag{2.33a}$$

$$\mathrm{Re}_d = \frac{1}{4}\mathrm{Re}_{D_h}\,\tilde{d}\tilde{u} \tag{2.33b}$$

Using equation (2.32), Taylor and Hodge (1993) displayed good agreement of skin friction predictions with experimental results over a wide range of uniform surface roughness shapes and distributions.

Completion of the solution requires the velocity profile to satisfy the global conservation of mass

$$\tilde{u}_m = 1 = 2\int_0^1 \beta_x \tilde{u}(1-\tilde{y})d\tilde{y} \tag{2.34a}$$

$$\tilde{u}_m = 1 = \int_0^1 \beta_x \tilde{u} d\tilde{y} \tag{2.34b}$$

The following procedure is presented by Taylor and Hodge (1993). Given the Reynolds number and the relative roughness parameters ( $\tilde{d}_0$, $\tilde{k}$, $\tilde{l}$, $\tilde{L}$ ), a solution for $f_f$ and $\tilde{u}(y)$ can be reached by:

1.) Assuming a value of $f_f$ and compute $\tilde{u}(y)$ using a finite difference procedure.

2.) Finding values of $f_f$ such that the corresponding values of $\tilde{u}_m$ bound 1.

3.) Using the method of false position to solve for $f_f$ such that $\tilde{u}_m = 1$.

The eddy viscosity relationship, $\mu_T / \mu$, and the velocity profile, $\tilde{u}(y)$, determined in the momentum equation are used in the solution of the energy equation. For the energy equation, the eddy conductivity parameter, L**, is defined as

$$L^{**} = \tilde{r}\beta_y\left(1+\frac{K_T}{K}\right) = \tilde{r}\beta_y\left(1+\frac{\mu_T}{\mu}\frac{\mathrm{Pr}}{\mathrm{Pr}_T}\right) \tag{2.35a}$$

$$L^{**} = \beta_y\left(1+\frac{K_T}{K}\right) = \beta_y\left(1+\frac{\mu_T}{\mu}\frac{\mathrm{Pr}}{\mathrm{Pr}_T}\right) \tag{2.35b}$$

The temperature profile, $\tilde{\theta}$, is defined such that

$$\tilde{\theta} = \frac{\theta}{Nu} \tag{2.36}$$

Substituting into the energy equation with the constant wall heat flux boundary condition gives

$$\tilde{\theta}'' + \frac{L^{**\prime}}{L^{**}}\tilde{\theta}' - Nu_d\,\frac{\pi\tilde{\theta}}{\tilde{l}\tilde{L}L^{**}} + \beta_x\,\frac{\tilde{u}(1-\tilde{y})}{L^{**}} = 0 \tag{2.37a}$$

$$\tilde{\theta}'' + \frac{L^{**\prime}}{L^{**}}\tilde{\theta}' - Nu_d\,\frac{\pi\tilde{\theta}}{\tilde{l}\tilde{L}L^{**}} + \beta_x\,\frac{\tilde{u}}{4L^{**}} = 0 \tag{2.37b}$$

with the boundary conditions

$$\tilde{y} = 0 : \tilde{\theta} = 0 \qquad (2.38)$$

$$\tilde{y} = 1 : \tilde{\theta}' = 0$$

From Kays and Crawford (1993), the turbulent Prandtl number is taken to be constant

$$\mathrm{Pr_T} = 0.9 \quad \mathrm{Pr} < 1 \qquad (2.39)$$

$$\mathrm{Pr_T} = 1.0 \quad \mathrm{Pr} > 1$$

Following Hosni et al. (1989) and Taylor et al. (1984), the local element Nusselt number is defined as a function of the local element Reynolds number as

$$Nu_d = 1.7\,\mathrm{Re}_d^{\,0.49}\,\mathrm{Pr}^{0.4}; \quad \mathrm{Re}_d \prec 2{,}500 \qquad (2.40)$$

$$Nu_d = 0.963\,\mathrm{Re}_d^{\,0.6}\,\mathrm{Pr}^{0.4}; \quad 2{,}500 \le \mathrm{Re}_d \prec 200{,}000$$

$$Nu_d = 0.06\,\mathrm{Re}_d^{\,0.84}\,\mathrm{Pr}^{0.4}; \quad \mathrm{Re}_d \ge 200{,}000$$

In addition to the local roughness element drag coefficient relationship, the local roughness Nusselt number relationship is a roughness model calibration developed for boundary-layer flows. Both are used unchanged within this work for fully-developed flows.

A solution for the temperature profile, $\tilde{\theta}$, can be achieved by applying the same finite difference procedure used in the momentum equation solution to equation (2.37). Determination of the Nusselt number requires the mean value of the nondimensional temperature to be equal to 1.

$$\theta_m = Nu\tilde{\theta}_m = 1 = 2\int_0^1 \beta_x \tilde{u}(1-\tilde{y})\tilde{\theta}d\tilde{y} \qquad (2.41a)$$

$$\theta_m = Nu\tilde{\theta}_m = 1 = \int_0^1 \beta_x \tilde{u}\,\tilde{\theta}d\tilde{y} \qquad (2.41b)$$

The solution for the energy equation with the constant wall temperature boundary condition is not as easily achieved. An iterative procedure is necessary. Utilizing the previously defined model for the eddy viscosity parameter, changes the energy equation with the constant wall temperature boundary condition to

$$\tilde{\theta}'' + \frac{L^{**\prime}}{L^{**}}\tilde{\theta}' - Nu_d \frac{\pi\tilde{\theta}}{\tilde{l}\tilde{L}L^{**}} + \beta_x \frac{\tilde{u}(1-\tilde{y})}{L^{**}}\theta = 0 \tag{2.42a}$$

$$\tilde{\theta}'' + \frac{L^{**\prime}}{L^{**}}\tilde{\theta}' - Nu_d \frac{\pi\tilde{\theta}}{\tilde{l}\tilde{L}L^{**}} + \beta_x \frac{\tilde{u}}{4L^{**}}\theta = 0 \tag{2.42b}$$

with the boundary conditions

$$\tilde{y} = 0:\ \tilde{\theta} = \theta = 0 \tag{2.43}$$

$$\tilde{y} = 1:\ \tilde{\theta}' = \theta' = 0$$

An iterative procedure is necessary because the equation now contains $\theta$. An initial profile is assumed for $\theta = \theta^*_1$. The energy equation is then modified to be

$$\tilde{\theta}_1'' + \frac{L^{**\prime}}{L^{**}}\tilde{\theta}_1' - Nu_d \frac{\pi\tilde{\theta}_1}{\tilde{l}\tilde{L}L^{**}} + \beta_x \frac{\tilde{u}(1-\tilde{y})}{L^{**}}\theta^*_1 = 0 \tag{2.44a}$$

$$\tilde{\theta}_1'' + \frac{L^{**\prime}}{L^{**}}\tilde{\theta}_1' - Nu_d \frac{\pi\tilde{\theta}_1}{\tilde{l}\tilde{L}L^{**}} + \beta_x \frac{\tilde{u}}{4L^{**}}\theta^*_1 = 0 \tag{2.44b}$$

and a solution for $\tilde{\theta}_1$ is achieved by using the same finite difference method used in the solutions of the momentum equation and the energy equation with the constant wall heat flux boundary condition. The Nusselt number is then computed as a function of $\theta_m$

$$Nu_1 = \frac{1}{\tilde{\theta}_{1,m}} \tag{2.45}$$

The process is repeated until a constant Nusselt number value is obtained using $\theta^*_i = Nu_{i-1}\tilde{\theta}_{i-1}$.

# CHAPTER III

# RANDOM ROUGHNESS ADAPTATIONS TO THE DISCRETE-ELEMENT MODEL

The discrete-element model has been validated for turbulent boundary layers over surfaces roughened with ordered, uniform elements (Hosni *et al*., 1989, 1991). In addition, McClain (2002) demonstrated excellent agreement between discrete-element method predictions and experimental results for turbulent boundary-layer flow over randomly-rough surfaces. Taylor and Hodge (1993) validated the method used within this work for predicting fully-developed Nusselt numbers and friction factors in pipes with ordered, uniform roughness elements. The Taylor and Hodge (1993) method is adapted to consider randomly-roughened surfaces using McClain's (2002) model.

Unlike the ordered surfaces used to validate the discrete-element model, randomly-rough surfaces are significantly different. Randomly-rough surfaces are characterized by roughness elements varying in shape, distribution, and height. The hemisphere or conical roughness elements previously considered have a circular cross-section at every elevation. For a randomly-rough surface, this is no longer true. Randomly-rough surfaces are also differentiated by the lack of an obvious reference surface on which to apply the "no-slip" condition for solving the differential equations. In contrast, the "no-slip" condition for ordered roughness elements is apparent because the elements are placed on a flat surface. These characteristics of randomly-rough

surfaces are evident in Figure 3.1, a three-dimensional profilometer trace of a randomly-rough surface.

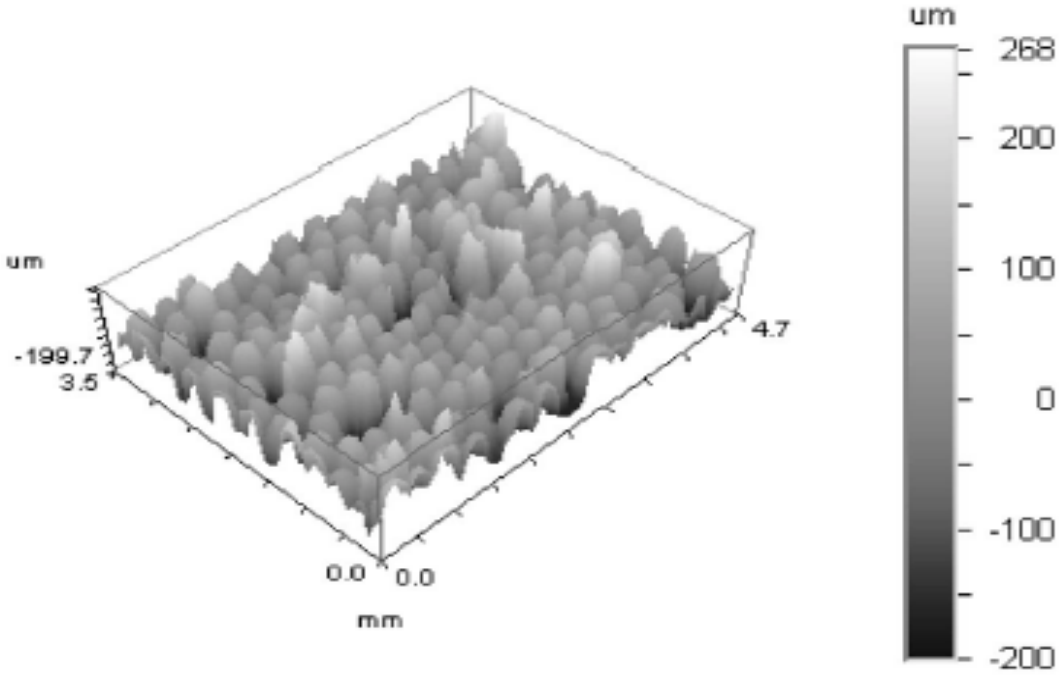


Figure 3.1 Three-dimensional Profilometer Trace of a Randomly-rough Surface (van Rij *et al.* 2002)

The discrete-element model requires blockage factors and element diameters for each roughness element at any y-location in the solution process. Use of a three-dimensional profilometer allows for the direct measurement of the surface features of a randomly-rough surface. From the three-dimensional profilometer characterization, the blockage factors and element diameters can be acquired. The differential equations presented in the previous chapter for ordered, uniform roughness elements are modified, according to the McClain (2002) model, to consider the actual surface traits.

When evaluating a deterministic surface with the discrete-element model, the reference surface is obvious. However, a randomly-rough surface does not present such

an easily distinguishable location. McClain (2002) uses the “melt down” surface as his reference surface. The “melt down” surface is described as the resulting surface if all individual roughness elements were melted and then solidified as a single volume with a constant height. Taylor (1983) demonstrated that the discrete-element predictions for closely-packed hemispheres agreed best when the “melt down” height was used as the reference surface.

Figure 3.2 shows the roughness elements for a randomly-rough surface at an elevation of 60% of the minimum valley to the maximum surface height. For this particular surface, the flow is from top to bottom. The areas blocked by flow are shown in black, while the white area represents the area open to flow. Examination of Figure 3.2 demonstrates that random roughness elements are not in general circular. The fact that the roughness elements appear elongated in the direction of the flow is also noted. Figure 3.3 examines the similarities between a random roughness element and an elliptical roughness element elongated in the direction of the flow.

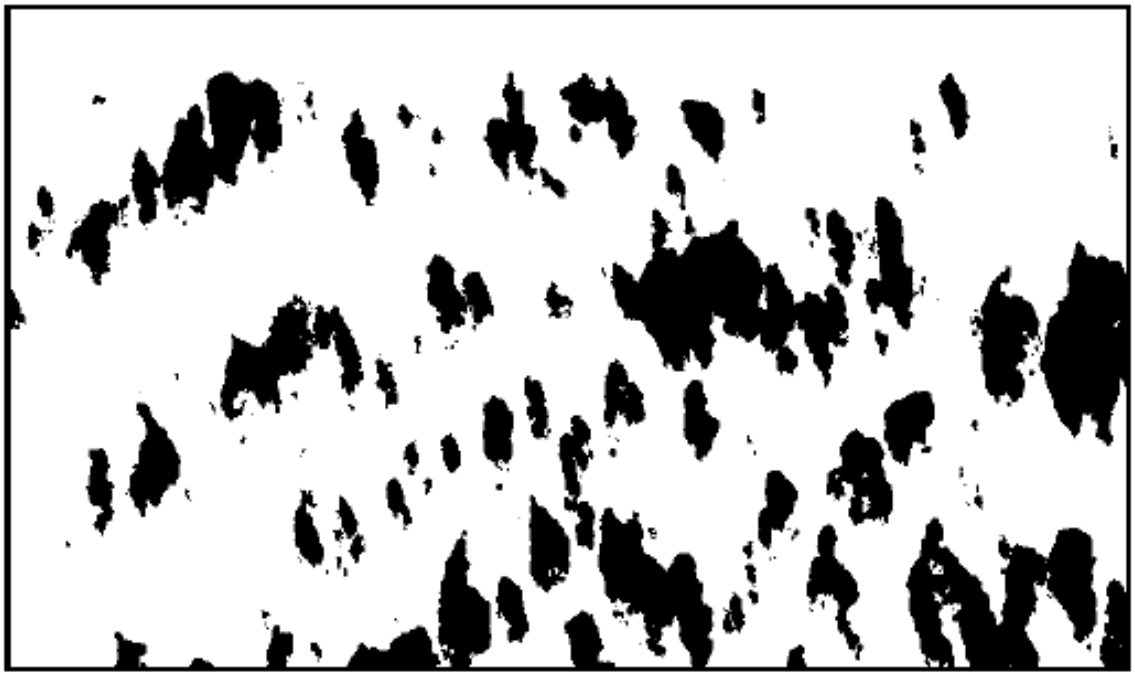

Figure 3.2 Randomly-rough Surface Blockage at 60% Elevation (McClain 2002)

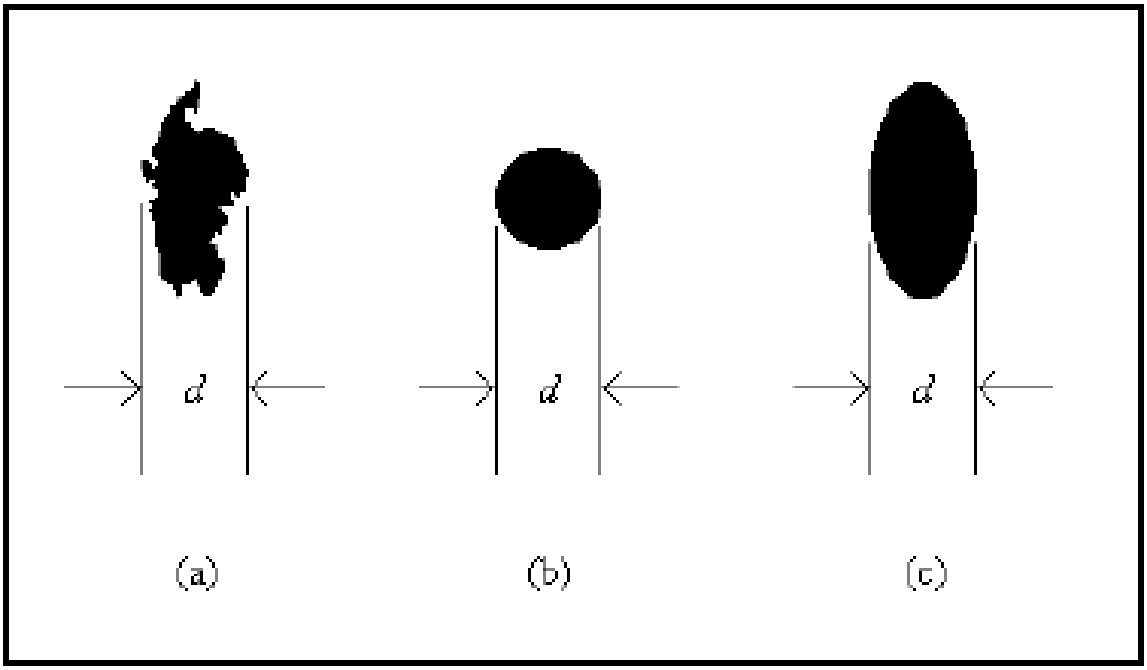


Figure 3.3 Example Roughness Element Representation: (a) Actual Randomly-rough Element, (b) Circular Roughness Element with the Same Transverse Width, (c) Elliptical Element with the Same Transverse Width and Eccentricity (McClain 2002)

The elliptical-like characteristics of the roughness elements led McClain (2002) to incorporate an eccentricity factor in the discrete-element model. An ellipsoidal blockage element elongated in the direction of the flow is displayed in Figure 3.4. The eccentricity factor, $\varepsilon$, is the ratio of the maximum width of the roughness element perpendicular to the flow to the maximum length of the roughness element parallel to the flow.

$$\varepsilon = \frac{2a}{2b} = \frac{a}{b} \tag{3.1}$$

The maximum width of the roughness element and the eccentricity factor are used to calculate the local drag and heat transfer for use in the discrete-element model.

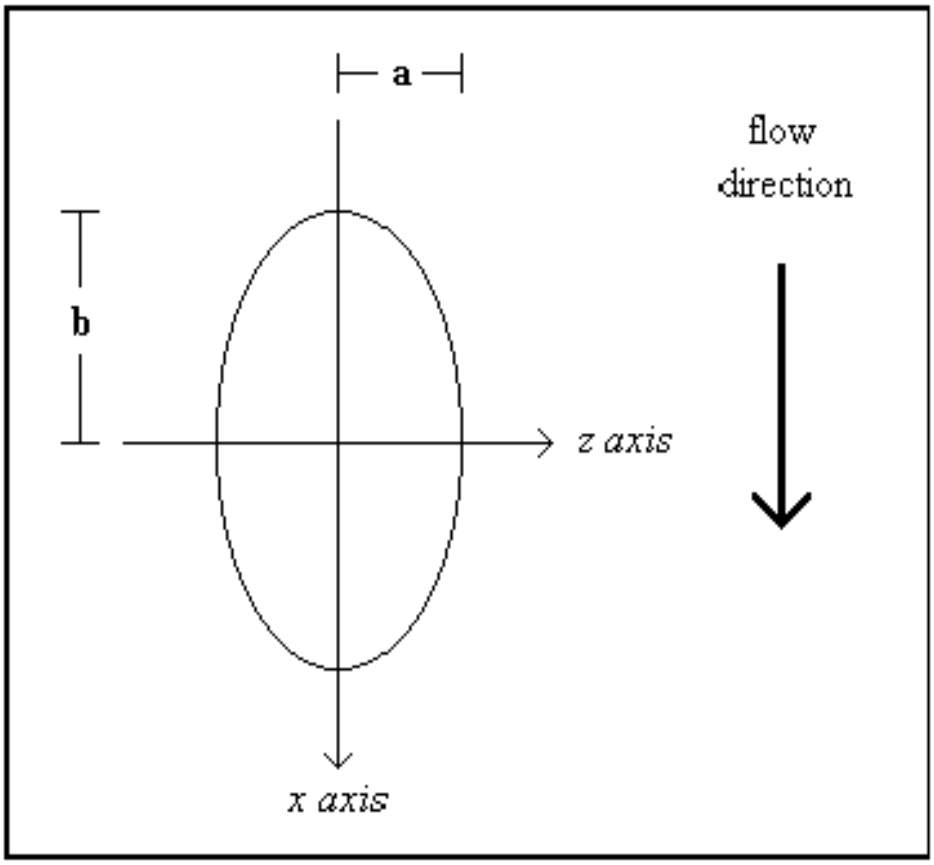


Figure 3.4 An Elliptical Roughness Element (McClain 2002)

McClain (2002) implements an ellipsoidal-blockage-element drag function due to the differences in the circular and ellipsoidal blockage elements. The circular-blockage-element drag function, equation (2.32), is modified to represent the differing drag characteristics. The ellipsoidal drag function is presented in equation (3.2).

$$C_D = \left(\frac{\mathrm{Re}_d}{1000}\right)^{-0.125} \varepsilon^{0.73456};\ \mathrm{Re}_d < 60{,}000 \text{ and } \varepsilon < 4.46 \tag{3.2}$$

$$C_D = 0.6\varepsilon^{0.73456};\ \mathrm{Re}_d > 60{,}000 \text{ and } \varepsilon < 4.46$$

For eccentricities greater than 4.46, the drag coefficients are described by the following equation.

$$C_D = 3.0\left(\frac{\mathrm{Re}_d}{1000}\right)^{-0.125};\ \mathrm{Re}_d < 60{,}000 \text{ and } \varepsilon > 4.46 \tag{3.3}$$

$$C_D = 1.8;\ \mathrm{Re}_d > 60{,}000 \text{ and } \varepsilon > 4.46$$

As the eccentricity increases, equation (3.3) captures the behavior of a flat plate perpendicular to the flow.

In addition to the differing drag characteristics, the McClain (2002) elliptical-discrete-element model also considers the increased surface area for element heat transfer for the elliptical elements, as compared to the circular element. An elliptical element area correction factor, $K_\varepsilon$, is defined as

$$K_\varepsilon = \left[\frac{1}{2}\left(1+\frac{1}{\varepsilon^2}\right) - \frac{1}{8.8}\left(1-\frac{1}{\varepsilon}\right)^2\right]^{\frac{1}{2}} \tag{3.4}$$

The elliptical element area correction factor is derived directly from the approximation of the perimeter of an ellipse. The additional surface area consideration increases the accuracy of the heat transfer information.

The steady, fully-developed, Reynolds averaged, two-dimensional turbulent momentum equations with random roughness for flow in a circular pipe or between infinite parallel plates are represented by the following differential equations.

$$0 = \frac{\mu}{r}\frac{d}{dy}\left[r\beta_y\left(1+\frac{\mu_T}{\mu}\right)\frac{\partial u}{\partial y}\right] - \beta_x\frac{dP}{dx} - \frac{1}{2}\rho u^2\frac{R}{rlL}\sum_{i=1}^{N_r} C_{D,i}d(y)_i \tag{3.5a}$$

$$0 = \mu\frac{d}{dy}\left[\beta_y\left(1+\frac{\mu_T}{\mu}\right)\frac{\partial u}{\partial y}\right] - \beta_x\frac{dP}{dx} - \frac{1}{2}\rho u^2\frac{1}{lL}\sum_{i=1}^{N_r} C_{D,i}d(y)_i \tag{3.5b}$$

The steady, fully developed, Reynolds averaged, two-dimensional turbulent energy equations with random roughness are

$$0 = \rho c_p\beta_x ur\frac{\partial T}{\partial x} - K\frac{\partial}{\partial y}\left[r\beta_y\left(1+\frac{K_T}{K}\right)\frac{\partial T}{\partial y}\right] - K\frac{\pi R}{lL}(T_0 - T)\sum_{i=1}^{N_r} K_{\varepsilon,i}Nu_{d,i} \tag{3.6a}$$

$$0 = \rho c_p\beta_x u\frac{\partial T}{\partial x} - K\frac{\partial}{\partial y}\left[\beta_y\left(1+\frac{K_T}{K}\right)\frac{\partial T}{\partial y}\right] - K\frac{\pi}{lL}(T_0 - T)\sum_{i=1}^{N_r} K_{\varepsilon,i}Nu_{d,i} \tag{3.6b}$$

The spacing parameters, $l$ and L, are the streamwise and transverse dimensions of the three-dimensional profilometer trace. The number of roughness elements at each y-location is denoted by $N_r$. The boundary conditions for equations (3.5) and (3.6) are

$$y = y_{mdh} : u = 0,\ T = T_0 \tag{3.7a}$$

$$y = R : \frac{du}{dy} = 0,\ \frac{\partial T}{\partial y} = 0$$

$$y = y_{mdh} : u = 0,\ T = T_0 \tag{3.7b}$$

$$y = h : \frac{du}{dy} = 0,\ \frac{\partial T}{\partial y} = 0$$

where $y_{mdh}$ is the “melt down” height.

In reality, random roughness elements are neither circular nor elliptical. However, reviewing Figure 3.3 visually demonstrates the similarities between a random

element and an elliptical element in comparison with a random element and a circular element. Using elliptical characteristics in the discrete-element model, McClain (2002) drastically improved the predictions when considering randomly-rough surfaces.

Successful predictions using the discrete-element model for randomly-rough surfaces requires characterization of the surface. The McClain (2002) technique for randomly-rough surface characterization is used. Using the output from a three-dimensional profilometer, the randomly-rough surface is characterized by evaluating the blockage fraction and the diameters and eccentricities of each roughness element at twenty-one equally-spaced height levels. The first height level is taken at the "melt height."

From the randomly-rough surface evaluation, a text file is created for use within the computer program. The text file is formatted in the following way. First, the number of elements present at the first height level is presented followed by the blockage fraction at that same height level. After the blockage fraction, the diameter for each roughness element at the first height level is given. Finally, the eccentricity for each roughness element at the first height level follows. This arrangement is continued for each of the twenty-one height levels used in the evaluation process. A properly formatted text file is provided in Appendix A for reference.

As previously discussed, the "melt height" is used as the reference surface when evaluating a randomly-rough surface. Using the "melt height" when considering flows inside circular pipes presents a new problem. Figure 3.5 illustrates how the "melt height" affects the diameter of a circular pipe. The Reynolds number for flows inside circular pipes is based on the original diameter. However, when using the discrete-element for

predictive purposes the new "melt" diameter is used. In McClain's (2002) boundary-layer research this was not a consideration. The Reynolds number in a boundary-layer flow is based on the length of the plate, which is unaffected by the "melt height." To account for the Reynolds number incontinuity, the following relationship is established with the assumption that the mass flow rates are equal in the original and "melt" cases.

$$\mathrm{Re}_{melt} = \mathrm{Re}_{original}\left(\frac{D_{original}}{D_{melt}}\right) \tag{3.8}$$

Using the ratio of the velocities between the original and "melt" cases, the Reynolds number relationship becomes strictly a function of the diameters. For flows between infinite parallel plates, the Reynolds number is not affected.

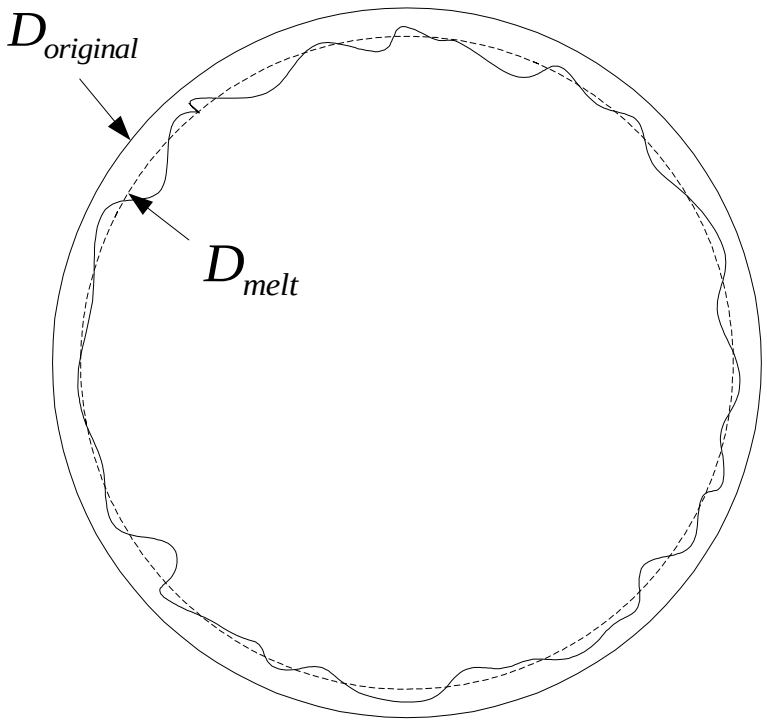


Figure 3.5 Circular Pipe with Random Roughness

# CHAPTER IV

# RESULTS AND DISCUSSION

This chapter presents friction factor and Nusselt number predictions from the discrete-element model computer program. Predictions are compared with classical, laminar and turbulent, smooth-wall results for flows within circular pipes and between infinite parallel plates. In addition to smooth-wall results, discrete-element model predictions are compared with experimental results for turbulent internal flows with deterministic surface roughness. Finally, predictions are presented for randomly-roughened surfaces inside circular pipes and between infinite parallel plates.

## Smooth Wall

Initially, the discrete-element model computer program was validated by comparison with the classic results for laminar and turbulent flows in circular pipes and between infinite parallel plates with smooth walls. Smooth-wall friction factor and Nusselt number predictions are made by specifying vanishingly-small roughness. Laminar flow is specified for cases where $Re < 2000$. Tables 4.1 and 4.2 compare the discrete-element model computer program predictions and the classic solutions (for example, Bejan, 1995) for laminar flows in smooth circular pipes and between smooth infinite parallel plates, respectively. The agreement for both of the friction factor solutions is excellent. The Nusselt number predictions are within 0.2% of the classic solutions.

Table 4.1 Laminar Flow Comparison in a Smooth Circular Pipe

| | Discrete-Element Model Predictions | | | Classic Solutions | | |
|---|---|---|---|---|---|---|
| $Re_D$ | $f_f$ | $Nu_H$ | $Nu_T$ | $f_f$ | $Nu_H$ | $Nu_T$ |
| 1000 | 0.016 | 4.364 | 3.65 | 0.016 | 4.364 | 3.66 |
| 2000 | 0.008 | 4.364 | 3.65 | 0.008 | 4.364 | 3.66 |

Table 4.2 Laminar Flow Comparison Between Smooth Infinite Parallel Plates

| | Discrete-Element Model Predictions | | | Classic Solutions | | |
|---|---|---|---|---|---|---|
| $Re_{Dh}$ | $f_f$ | $Nu_H$ | $Nu_T$ | $f_f$ | $Nu_H$ | $Nu_T$ |
| 1000 | 0.024 | 8.238 | 7.55 | 0.024 | 8.235 | 7.54 |
| 2000 | 0.012 | 8.238 | 7.55 | 0.012 | 8.235 | 7.54 |

Figure 4.1 shows the smooth-wall turbulent friction factor predictions as compared with the following empirical relation reported by Bejan (1995) for high Reynolds numbers in smooth tubes.

$$f_f = 0.046\,\mathrm{Re}_{D_h}^{-0.2} \tag{4.1}$$

Equation (4.1) holds for Reynolds numbers between $2 \times 10^4$ and $10^6$. The Nusselt number predictions are compared in Figure 4.2 with results from the Dittus-Boelter correlation. The Nusselt number predictions are a result of using a Prandtl number of 0.9 and the constant heat flux boundary condition. In the friction factor and Nusselt number comparisons, the results for flows inside circular pipes are followed by the results for flows between infinite parallel plates. For flows between parallel plates, the empirical correlations are based on the hydraulic diameter. In each figure, the empirical correlation is characterized by the solid line and the prediction is represented by the dashed line.

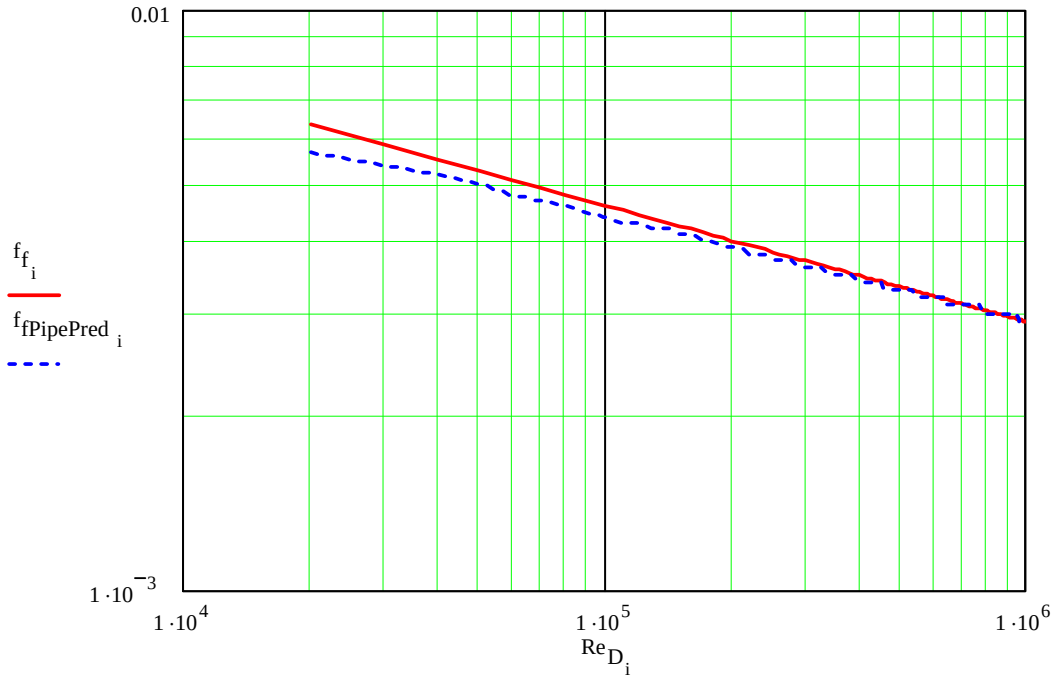


(a) Circular Pipe

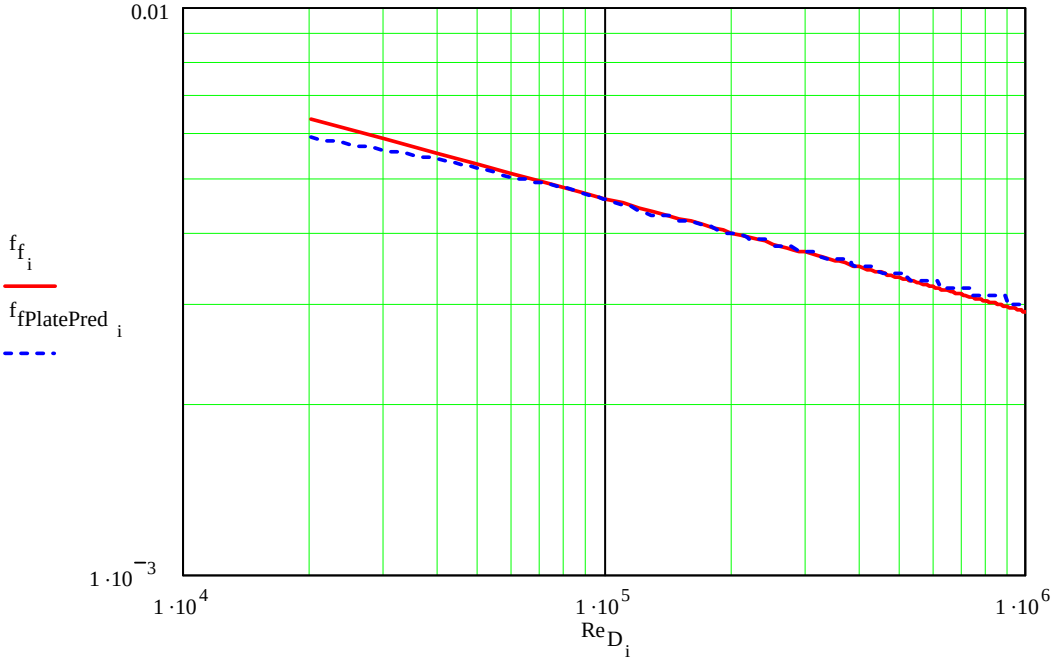


(b) Infinite Parallel Plates

Figure 4.1 Comparison of Empirical Correlation and Predicted Friction Factors for Flows in a (a) Circular Pipe and (b) between Infinite Parallel Plates

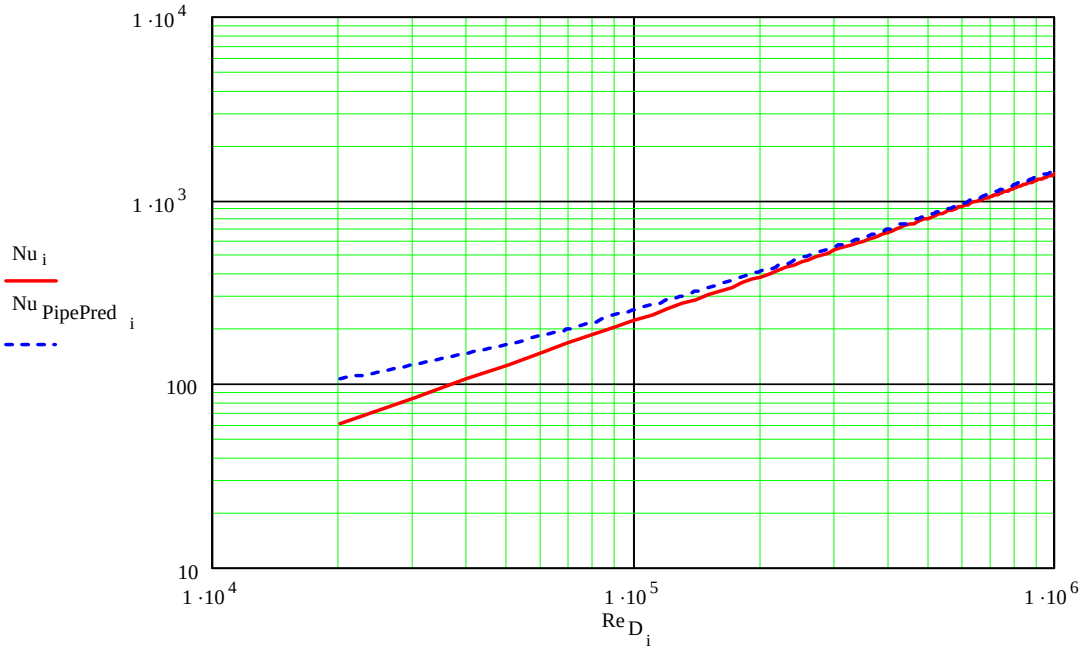


(a) Circular Pipe

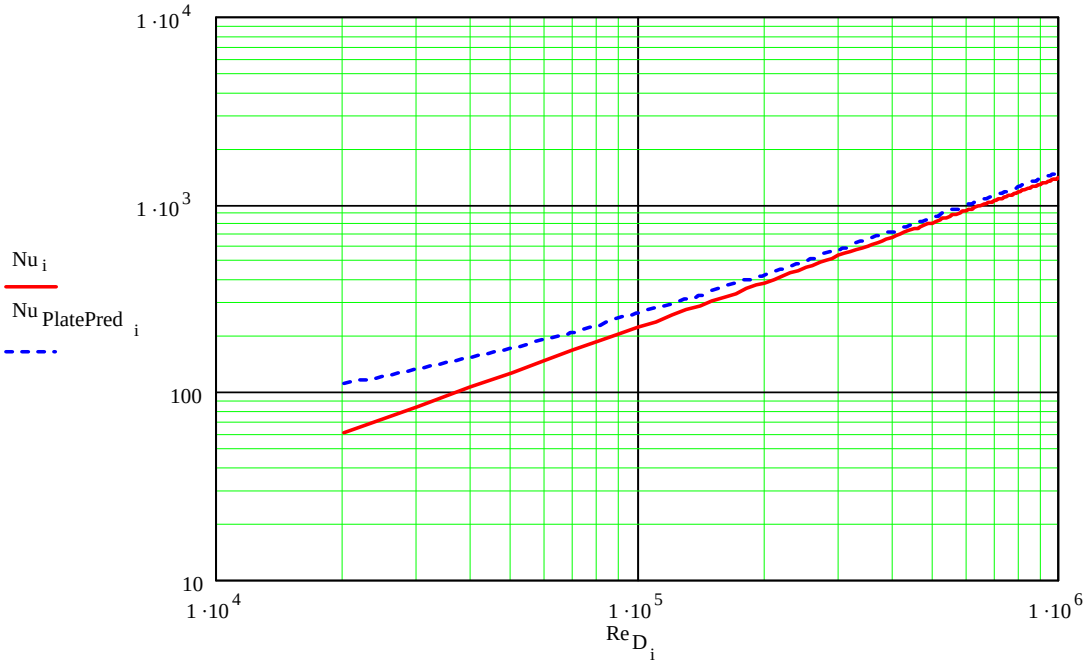


(b) Infinite Parallel Plates

Figure 4.2 Comparison of Empirical Correlation and Predicted Nusselt Numbers for Flows in a (a) Circular Pipe and (b) between Infinite Parallel Plates

The results exhibited by each figure display excellent agreement. Since the turbulence model used within the computer program was derived from smooth-wall turbulent flow data, these results were expected.

**Deterministic Roughness**

Scaggs (1987) experimentally measured friction factors for turbulent flow in pipes roughened with hemispheres and cones. He successfully measured the friction factor in pipes with a range of different roughness sizes and spacings. Table 4.3 describes four of the nine roughness patterns he used.

Table 4.3 Roughness Patterns of Scaggs (1987)

| Surface | Pipe Diameter [mm] | Element Base Diameter [mm] | Element Spacing [mm] | Element Height [mm] |
|---|---|---|---|---|
| Large Hemispheres | | | | |
| A-1 | 51.46 | 2.55 | 5.10 | 1.27 |
| A-2 | 51.56 | 2.55 | 10.20 | 1.27 |
| Small Hemispheres | | | | |
| B-1 | 51.88 | 1.25 | 2.50 | 0.65 |
| B-2 | 51.54 | 1.25 | 5.05 | 0.60 |

Figures 4.3 through 4.6 compare Scaggs (1987) experimentally-measured friction factors with the predicted values. In the figures, Scaggs experimental data points are represented by symbols and the predictions are represented by a solid line. There are no heat transfer comparisons because Scaggs did not present any heat transfer data. In all of the figures, the agreement is excellent. Conformity between the experimental and predicted values is expected. Taylor et al. (1984) calibrated the roughness model used

within this work using the cone and spherical segment data of Schlichting (1936). Scaggs et al. (1988), in turn, demonstrated excellent agreement with Taylor's results.

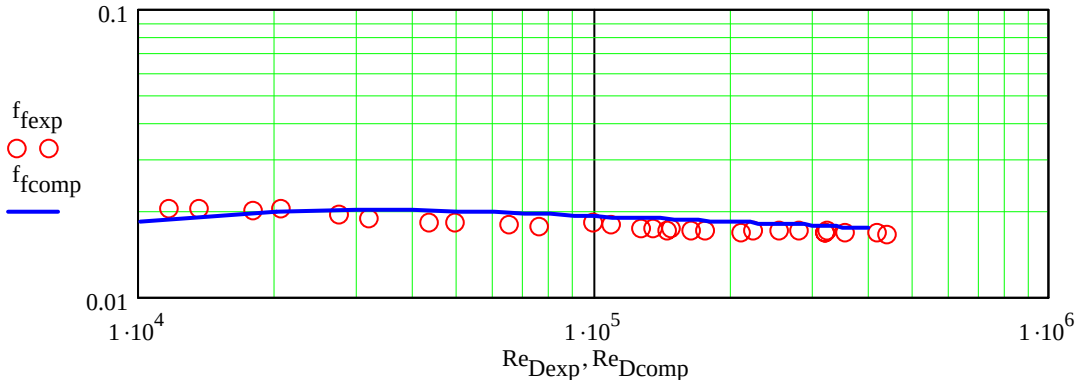


Figure 4.3 Comparison of Scaggs (1987) Experimental Results for Surface A-1 with Predicted Values

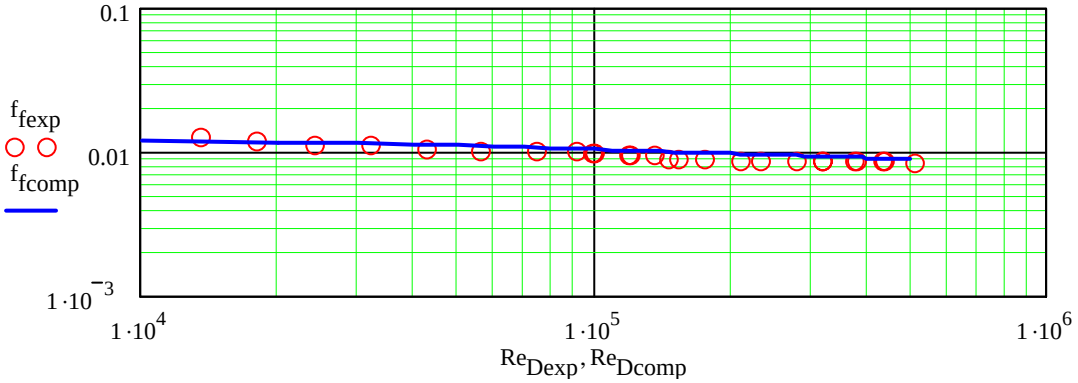


Figure 4.4 Comparison of Scaggs (1987) Experimental Results for Surface A-2 with Predicted Values

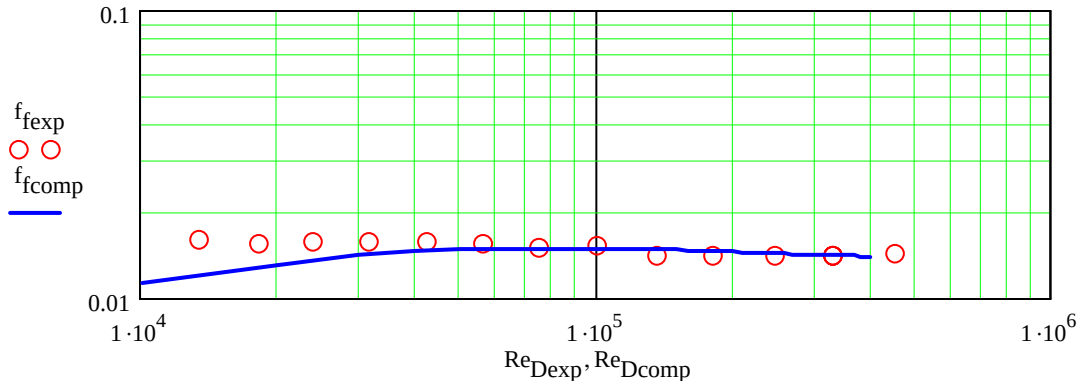


Figure 4.5 Comparison of Scaggs (1987) Experimental Results for Surface B-1 with Predicted Values

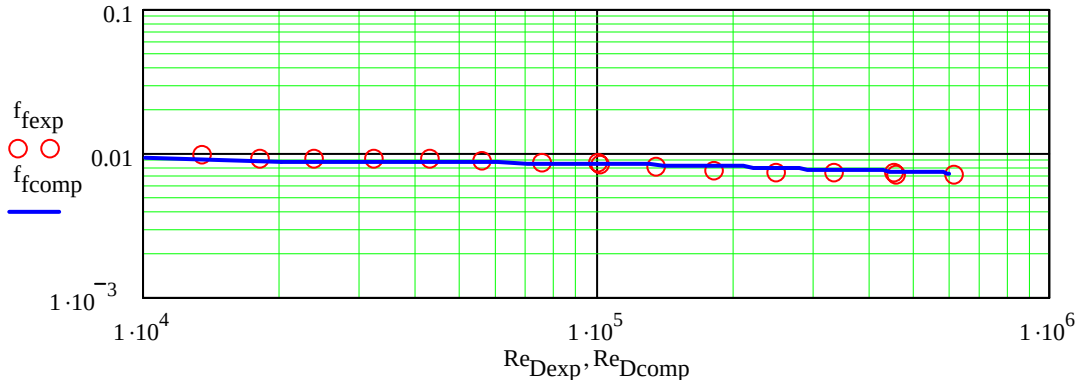


Figure 4.6 Comparison of Scaggs (1987) Experimental Results for Surface B-2 with Predicted Values

**Random Roughness**

To ensure the McClain (2002) method for characterizing a randomly-rough surface was properly implemented in the discrete-element model, a data set from Scaggs (1987) was used for comparison. Predictions for Surface A-1 were generated from the discrete-element model for deterministic roughness. In Figures 4.7 and 4.8, these deterministic results are compared with predictions from the discrete-element model after characterizing the same deterministic surface with the McClain method for randomly-rough surfaces. The deterministic method considers only the effect of a single roughness

element. However, when characterizing the surface with the McClain method, the spacing was expanded to include the average effect of four roughness elements. Using the McClain method of characterization forces the elemental spacing parameters to become the size of the surface considered since multiple roughness elements are considered. This is necessary because the transverse and parallel spacings are no longer constant with randomly-rough surfaces. The average effects of the roughness elements are considered when utilizing the McClain method of characterization.

In addition to friction factor data, Nusselt numbers are included since predictions are being compared. In each figure, the deterministic predictions are represented by symbols. The predictions from the McClain characterization method and the deterministic method are identical. These results demonstrate that the McClain method successfully replicates multiple deterministic roughness elements on a flat surface.

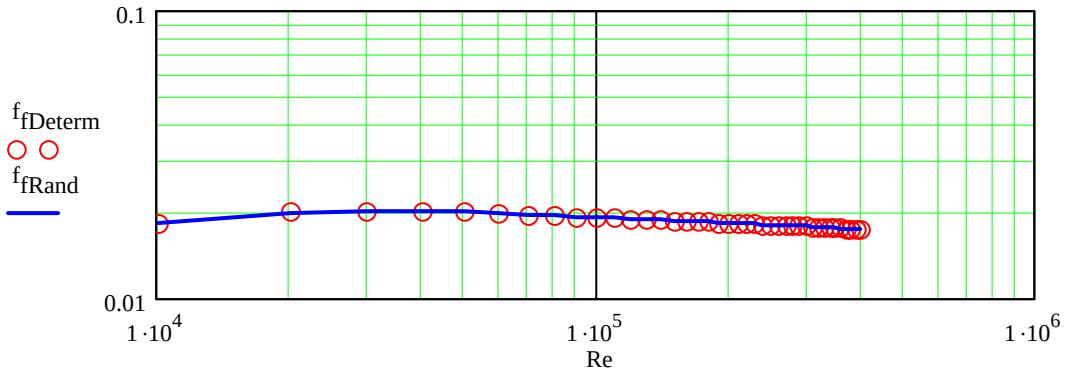


Figure 4.7 Comparison of Friction Factor Predictions Using the McClain Characterization Method and the Deterministic Method

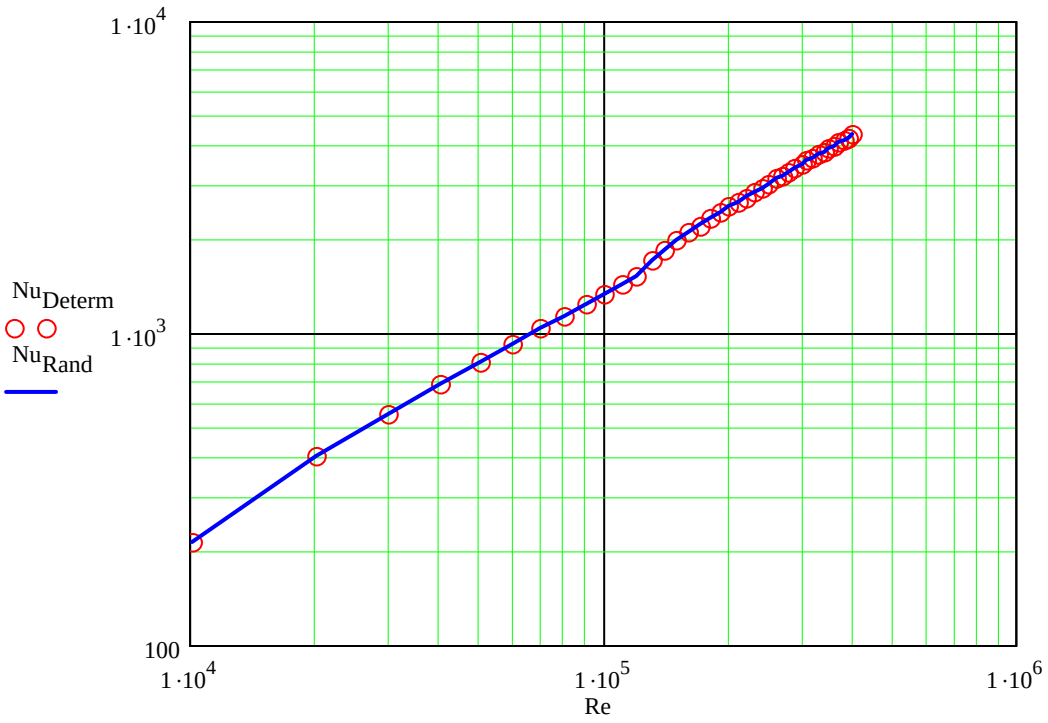


Figure 4.8 Comparison of Nusselt Number Predictions Using the McClain Characterization Method and the Deterministic Method

To guarantee that the "melt height" was correctly implemented in the discrete-element, the following comparison was used. Predictions were created for Surface A-1 with a "melt height" of 0.1669 mm. These predictions were then compared with predictions for Surface A-1 with a pipe diameter reduced by twice the "melt height." Since the flow effects below the "melt height" are considered negligible, the predictions should be identical. Comparisons between the two predictions are presented in Figures 4.9 and 4.10. The results are identical.

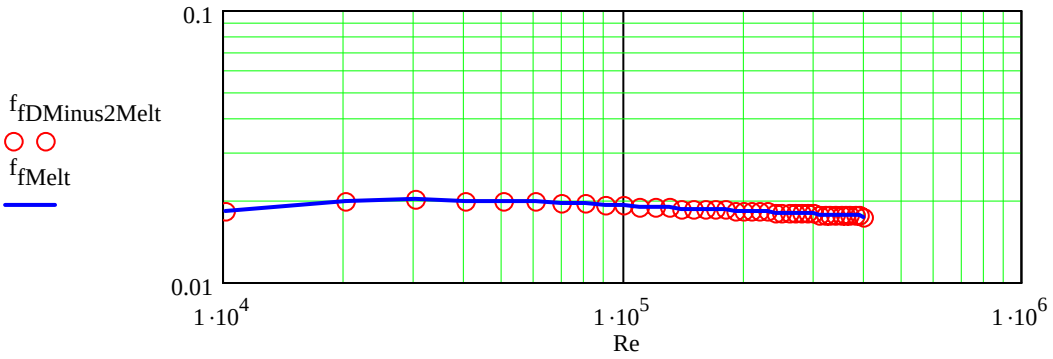


Figure 4.9 Comparison of Friction Factor Predictions for "Melt Height" Validation

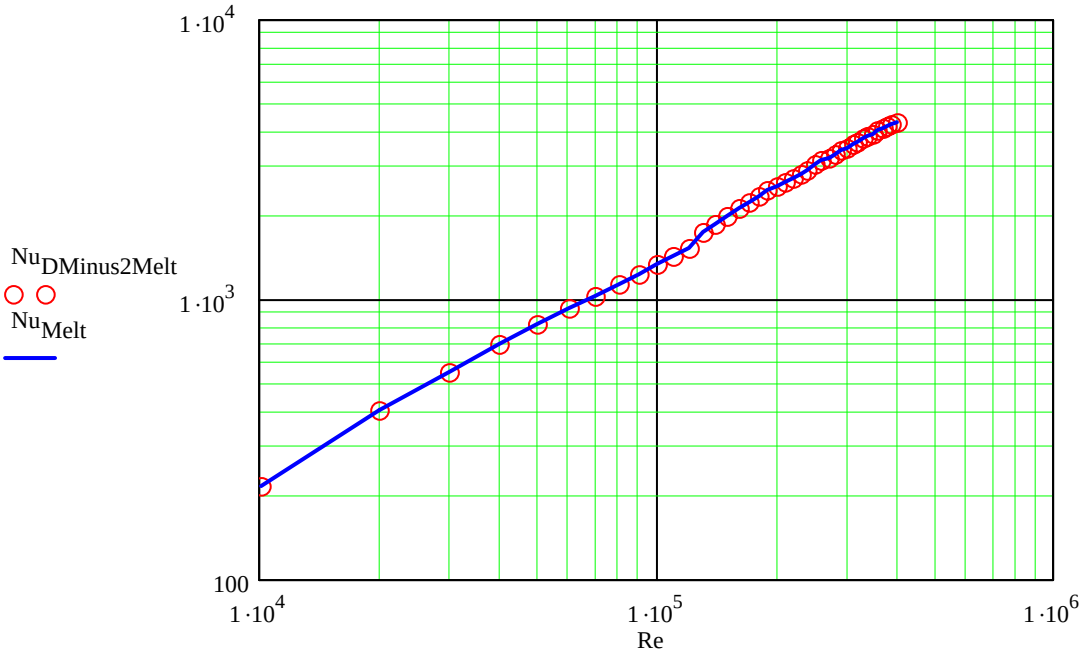


Figure 4.10 Comparison of Nusselt Number Predictions for "Melt Height" Validation

A noticeable change in slope is displayed at a Reynolds number of approximately $1.25 \times 10^5$ in Figure 4.10. The slope change is a result of the functional form of equation (2.40), the local roughness Nusselt number relationship. At the specified point, the local Reynolds moves from one function range to the next in a piecewise-continuous definition.

In Figures 4.11 through 4.14 the predictions are presented for the "deposit" surface presented in McClain (2002). The surface was treated as if it were the inside of a circular pipe or the interior of infinite parallel plates. The conditions used to achieve the predictions are displayed in Table 4.4. All of the conditions were arbitrarily chosen. The pipe diameter and Prandtl number were chosen to be consistent with that of Scaggs (1987). The Reynolds number range for the circular pipe predictions presented in Figures 4.11 and 4.12 are modified according to equation (3.8). This modification is necessary to account for the Reynolds number modification when using the "melt height" for internal flows. This modification is addressed in Chapter 3.

Table 4.4 Conditions for the "Deposit" Surface [McClain (2002)] Predictions

| Diameter or Plate Spacing [mm] | Transverse Length [mm] | Parallel Length [mm] | "Melt Height" [mm] | Prandtl Number |
|---|---|---|---|---|
| 51.46 | 50.0 | 50.0 | 1.5 | 6.2 |

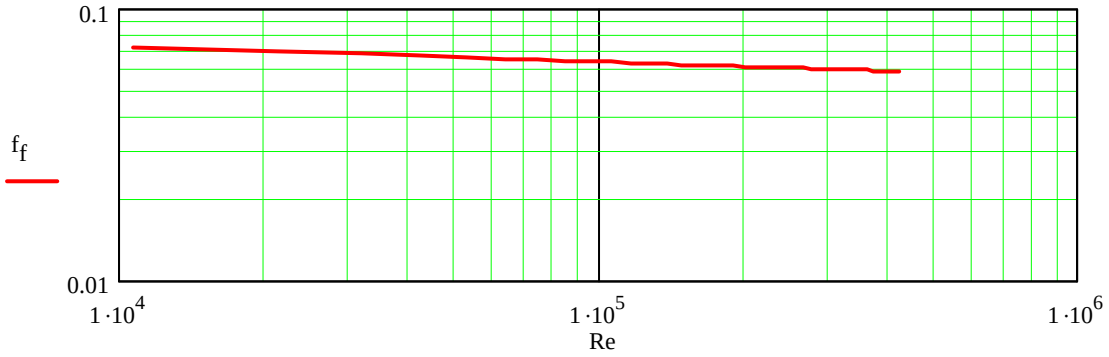


Figure 4.11 Friction Factor Predictions for the "Deposit" Surface [McClain (2002)] in a Circular Pipe

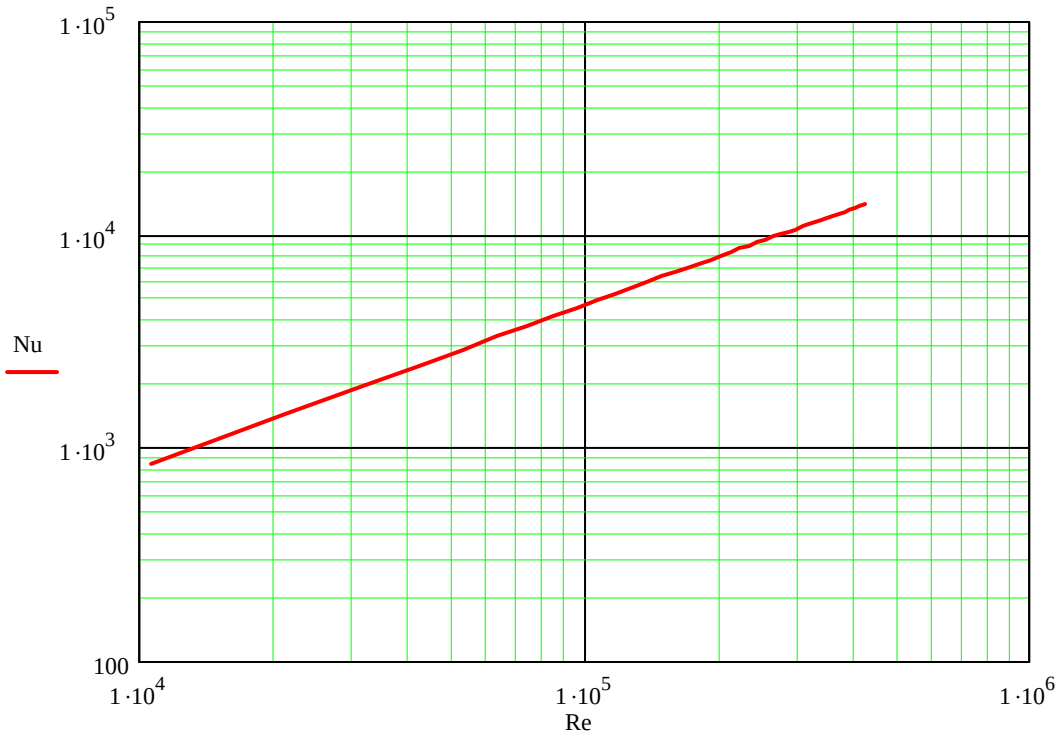


Figure 4.12 Nusselt Number Predictions for the "Deposit" Surface [McClain (2002)] in a Circular Pipe

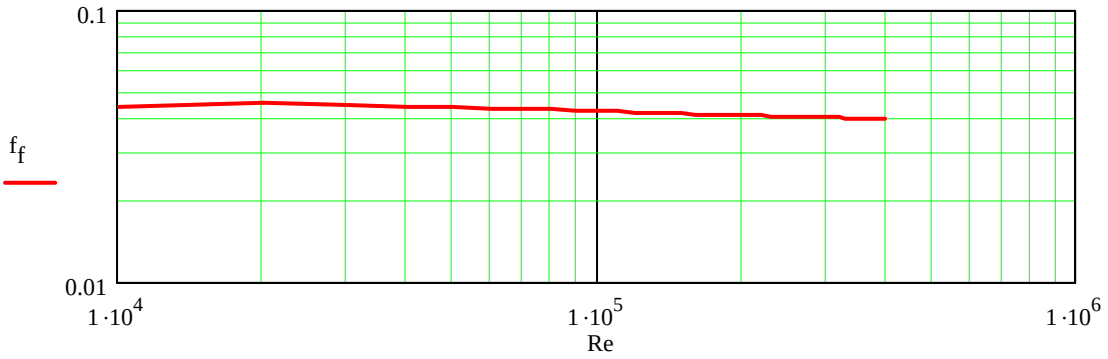


Figure 4.13 Friction Factor Predictions for the "Deposit" Surface [McClain (2002)] for Infinite Parallel Plates

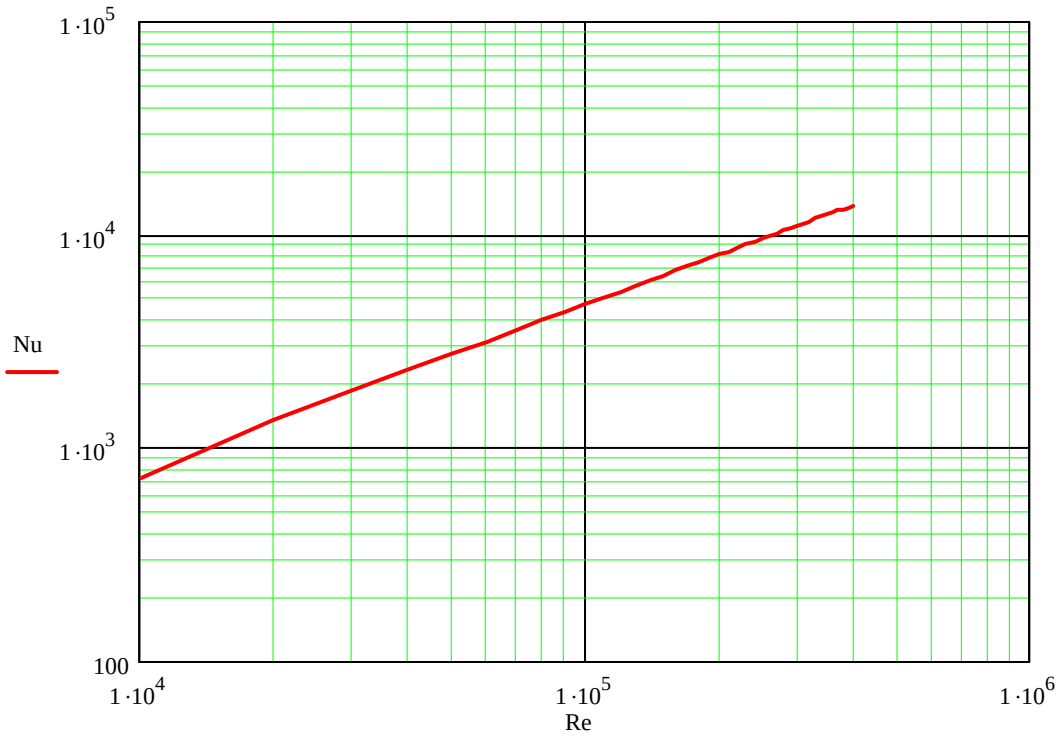


Figure 4.14 Nusselt Number Predictions for the "Deposit" Surface [McClain (2002)] for Infinite Parallel Plates

No experimental results are provided for comparison because current literature does not provide any experimental results for internal flows over randomly-rough surfaces *with the roughness geometry characterized by three-dimensional profilometer traces*. Velocity profiles for fully-developed, internal flows over randomly-rough, deterministically rough, and smooth surfaces are shown in Figure 4.15. The vertical axis of the figure is the nondimensional radius, r / R. The nondimensional velocity along the horizontal axis is nondimensionalized with respect to the centerline velocity. The solid line represents the velocity profile over the randomly-rough surface. The velocity profile over the deterministically rough surface is characterized by the dash-dot line. Finally, the dashed line represents the flow through the smooth pipe. A magnified view, close to the pipe wall, is provided in Figure 4.16 for the same three velocity profiles.

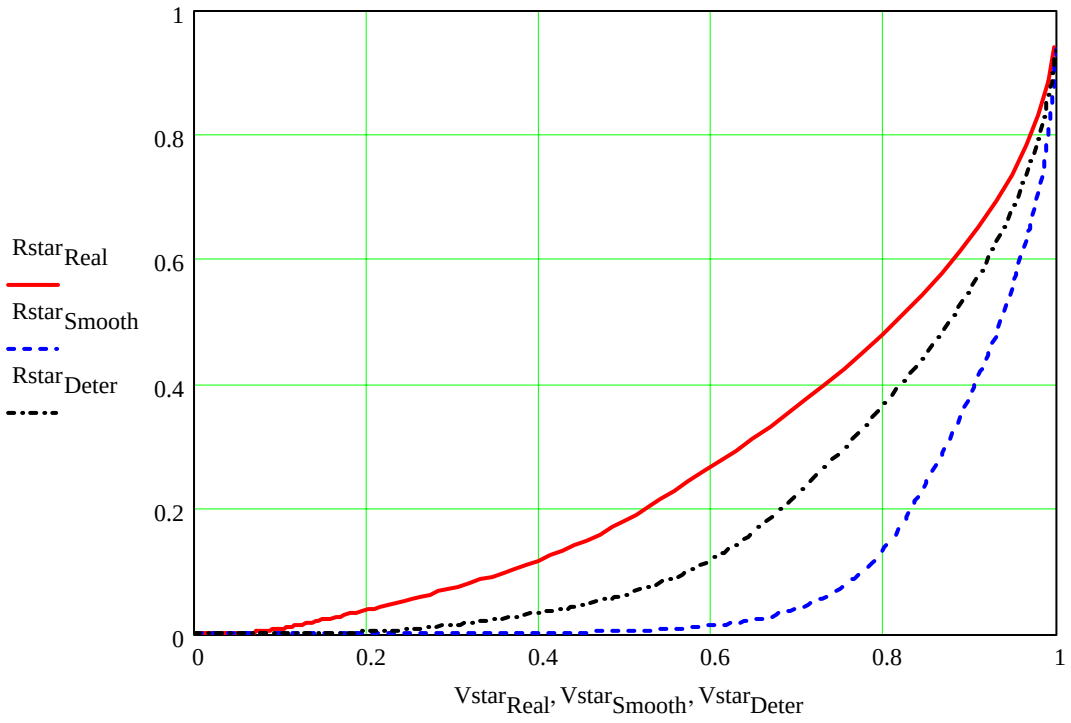


Figure 4.15 Internal Flow Velocity Profiles over Randomly-rough, Deterministically-rough, and Smooth Surfaces

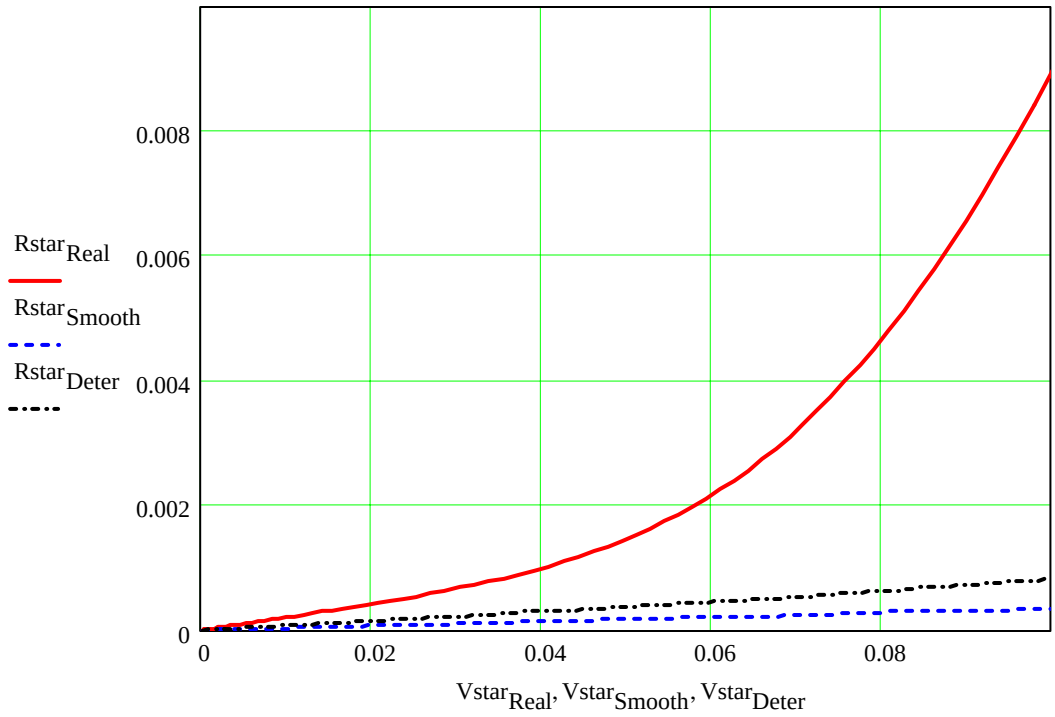


Figure 4.16 Magnified View of Internal Flow Velocity Profiles over Randomly-rough, Deterministically-rough, and Smooth Surfaces

The velocity profile over the randomly-rough surface has the greatest slope of the three profiles. The deterministically rough profile falls between the randomly-rough profile and the smooth wall profile. All of these results are expected. The randomly-rough surface is characterized by a large number of densely-packed roughness elements. This characteristic results in a much larger blockage factor as compared to those of the deterministic and smooth surfaces. In turn, the increased blockage forces the boundary layer, over the randomly-rough surface, further away from the pipe wall.

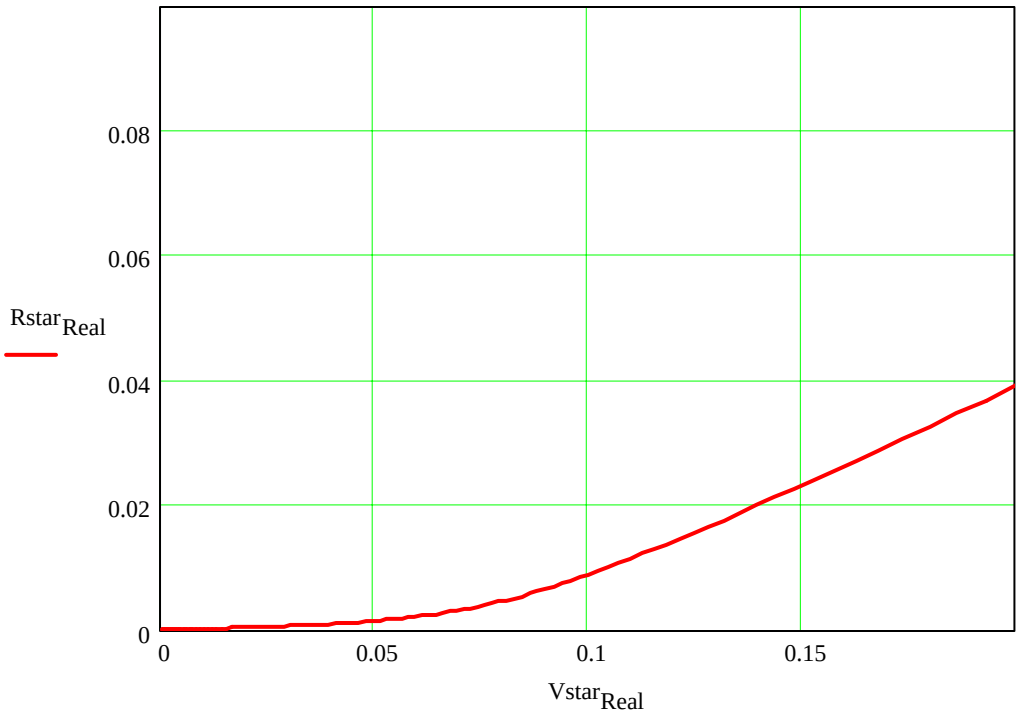


Figure 4.17 Internal Flow Velocity Profile over a Randomly-Rough Surface, Close to the Wall

The effects of the increased blockage of the randomly-rough surface are also evident in Figure 4.17. Figure 4.17 displays the velocity profile over the randomly-rough surface. The bottom 10% of the velocity profile is shown to display how the densely packed roughness elements of the randomly-rough surface affect the flow. At the "melt height" there is no significant flow. The flow reaches 10% of the centerline velocity at 1% of the radius. In comparison, at the same radial point the velocity of the deterministically-rough flow has reached almost 27% of the centerline velocity. The larger slope of the randomly-rough velocity profile is a result of the increased blockage close to the wall.

# CHAPTER V

# CONCLUSIONS

A discrete-element prediction method has been developed for fully-developed flows in a circular pipe and between infinite parallel plates with random surface roughness. The McClain (2002) method of characterization is used to successfully describe the randomly-rough surface for use within the discrete-element model.

Initially, discrete-element model predictions for laminar, smooth wall flows inside circular pipes and between infinite parallel plates were compared with classical solutions. Predictions were identical or within 0.2% of the classical solutions. Accepted experimental correlations for turbulent, internal, smooth wall flows were then compared with predictions. The agreement was excellent. Experimental friction factor data from four surfaces from Scaggs (1987) were also used for comparison. The experimental results were from deterministically-roughened circular pipes. Predictions from the model demonstrated excellent agreement with the experimental results.

Friction factor and Nusselt number predictions were also presented for fully-developed flows in circular pipes and between infinite parallel plates with randomly-rough surfaces. Comparisons were not provided due to the lack of experimental data in current literature. However, velocity profiles for flows over randomly-rough, deterministically-rough and smooth surfaces were provided for comparison. The expected results were realized. The velocity profile over the randomly-rough surface

exhibited a greater slope as compared to the deterministically-rough and smooth surface profiles.

Proper validation of this discrete-element prediction model for consideration of randomly-rough surfaces requires experimental data sets for comparison. Future works should include acquisition of experimental friction factors and Nusselt numbers for fully-developed flows inside circular pipes and between infinite parallel plates with randomly-rough surfaces with the roughness geometry characterized by three-dimensional profilometer traces. The randomly-rough surfaces must lend themselves to description by the McClain (2002) method of characterization.

# BIBLIOGRAPHY


Bejan, A., *Convective Heat Transfer*, New York: John Wiley & Sons, Inc., Second Edition, 1995.

Hosni, M. H., H. W. Coleman, and R. P. Taylor, "Measurement and Calculation of Surface Roughness Effects on Turbulent Flow and Heat Transfer," Report TFD-89-1, Department of Mechanical and Nuclear Engineering, Mississippi State University, 1989.

Kays, W. M. and M. E. Crawford, *Convective Heat and Mass Transfer*, New York: McGraw-Hill, Inc., Third Edition, 1993.

McClain, S. T., "A Discrete-Element Model for Turbulent Flow over Randomly-Rough Surfaces," Ph.D. Dissertation, Department of Mechanical Engineering, Mississippi State University, 2002.

Nikuradse, J., "Laws for Flows in Rough Pipes," *VDI-Forchungsheft 361*, Series B, Vol. 4, 1933, also as NACA TM 1292, 1950.

Scaggs, W. F., "Measurement and Prediction of Rough Wall Effects on Friction Factors in Turbulent Pipe Flow," Masters Thesis, Department of Mechanical and Nuclear Engineering, Mississippi State University, 1987.

Scaggs, W. F., R. P. Taylor, and H. W. Coleman, "Measurement and Prediction of Rough Wall Effects on Friction Factors in Turbulent Pipe Flow," Report TFD-88-1, Department of Mechanical and Nuclear Engineering, Mississippi State University, 1988.

Schlichting, H., "Experimental Investigation of the Problem of Surface Roughness," Ingenieur-Archiv, Vol. VII, No. 1, 1936, and NACA TM 823, 1937.

Taylor, R. P., "A Discrete Element Prediction Approach for Turbulent Flow over Rough Surfaces," Ph.D. Dissertation, Department of Mechanical and Nuclear Engineering, Mississippi State University, 1983.

Taylor, R. P., H. W. Coleman, and B. K. Hodge, "A Discrete Element Prediction Approach for Turbulent Flow Over Rough Surfaces," Report TFD-84-1, Department of Mechanical and Nuclear Engineering, Mississippi State University, 1984.

Taylor, R. P. and B. K. Hodge, "Validated Heat-Transfer and Pressure-Drop Prediction Methods Based on the Discrete Element Method: Phase 1, Three-Dimensional Roughness," Report ANL/ESD/TM-31, Argonne National Laboratory, 1992.

Taylor, R. P., and B. K. Hodge, "A Validated Procedure for the Prediction of Fully-Developed Nusselt Numbers and Friction Factors in Pipes with 3-Dimensional Roughness," *Journal of Enhanced Heat Transfer*, Vol. 1, No. 1, pp. 23-35, 1993.

Van Rij, J. A., B. J. Belnap, and P. M. Ligrani, "Analysis and Experiments on Three-Dimensional, Irregular Surface Roughness," *Journal of Fluids Engineering*, Vol. 124, pp. 671-677, 2002.

# APPENDIX A

# TEXT FILE FORMAT FOR EVALUATING RANDOMLY-ROUGH SURFACES

As stated in Chapter 3, proper characterization of a randomly-rough surface is required for successful predictions from the discrete-element model. Proper characterization requires correct formatting of the text file. The text file conveys the physical characteristics of the randomly-rough surface.

Using the output file from a three-dimensional profilometer, the randomly-rough surface is divided into twenty-one equally spaced height levels. The first level is assigned at the "melt height." The final level is taken at the pinnacle of the tallest roughness element. The blockage fraction and the diameters and eccentricity factors of each roughness element are evaluated at each height level.

From the randomly-rough surface evaluation, a text file with the following format is created. The number of elements present at the first height level is presented followed by the blockage fraction at that same height level. After the blockage fraction, the diameter for each roughness element at the first height level is given. Finally, the eccentricity for each roughness element at the first height level follows. This arrangement is continued for each of the twenty-one levels.

Figure A.1 shows a layout of Scaggs (1987) Surface A-1. Following Figure A.1, an example of a properly formatted text file for Scaggs Surface A-1 utilizing the McClain method of characterization is provided. In Figure A-1, the area within the dashed box is the region under consideration in the example. Comments are provide for better understanding.

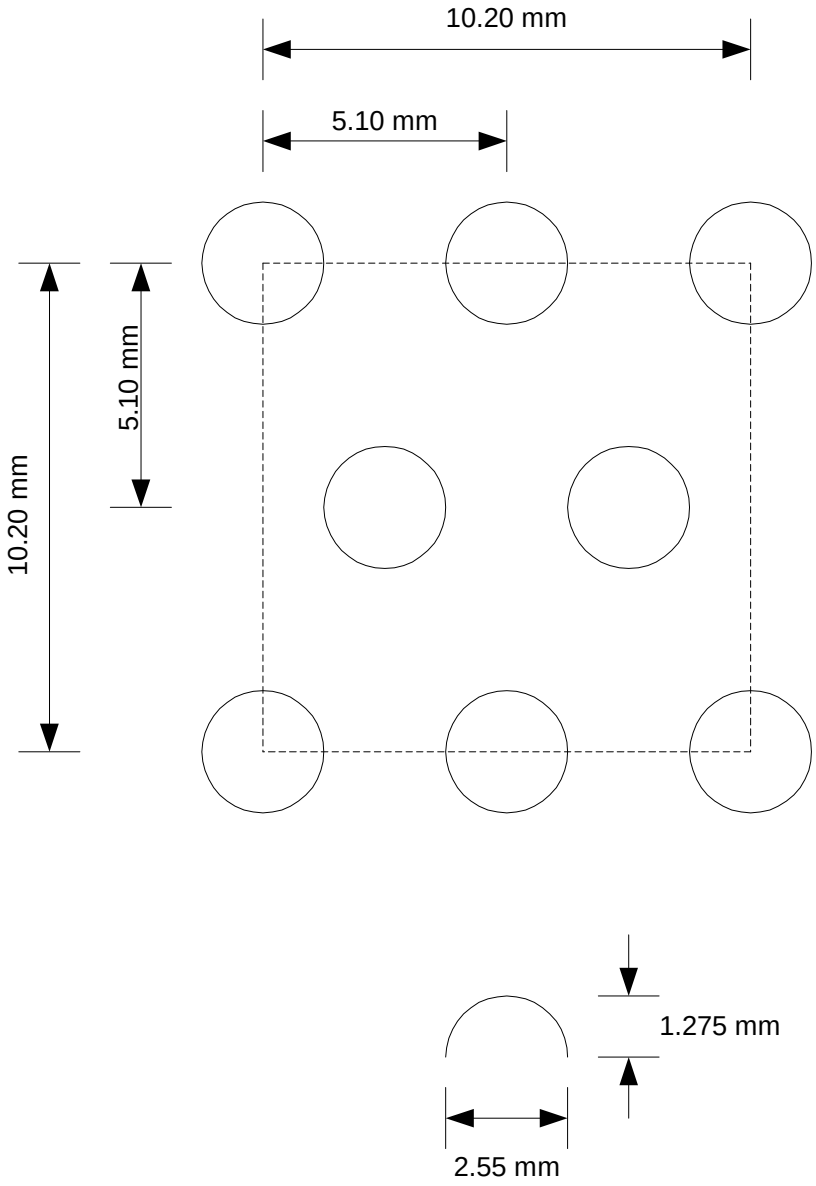


Figure A.1 Description of Scaggs (1987) Surface A-1 Utilizing the McClain (2002) Method of Characterization

| | | |
|---|---|---|
| 4 | ← | Number of roughness elements at the first height level. |
| 0.196349375 | | Blockage fraction, $1-\beta$, at the first height level. |
| 2.55 | | Diameter for roughness element #1 (mm) |
| 2.55 | | Diameter for roughness element 2 |
| 2.55 | | Diameter for roughness element #3 |
| 2.55 | | Diameter for roughness element #4 |
| 1.0 | | Eccentricity factor for roughness element #1 |
| 1.0 | | Eccentricity factor for roughness element #2 |
| 1.0 | | Eccentricity factor for roughness element #3 |
| 1.0 | | Eccentricity factor for roughness element #4 |
| 4 | ← | Number of roughness elements at the second height level. |
| 0.195858502 | | Blockage fraction, $1-\beta$, at the second height level. |
| 2.546811 | | Diameter for roughness element #1 (mm) |
| 2.546811 | | Diameter for roughness element #2 |
| 2.546811 | | Diameter for roughness element #3 |
| 2.546811 | | Diameter for roughness element #4 |
| 1.0 | | Eccentricity factor for roughness element #1 |
| 1.0 | | Eccentricity factor for roughness element #2 |
| 1.0 | | Eccentricity factor for roughness element #3 |
| 1.0 | | Eccentricity factor for roughness element #4 |
| 4 | | |
| 0.194385881 | | |
| 2.537218 | | |
| 2.537218 | | |
| 2.537218 | | |
| 2.537218 | | |
| 1.0 | | |
| 1.0 | | |
| 1.0 | | |
| 1.0 | | |
| 4 | | |
| 0.191931514 | | |
| 2.521149 | | |
| 2.521149 | | |
| 2.521149 | | |
| 2.521149 | | |
| 1.0 | | |
| 1.0 | | |
| 1.0 | | |
| 1.0 | | |
| 4 | | |
| 0.1884954 | | |
| 2.49848 | | |
| 2.49848 | | |
| 2.49848 | | |
| 2.49848 | | |

1.0
1.0
1.0
1.0
4
0.184077539
2.469027
2.469027
2.469027
2.469027
1.0
1.0
1.0
1.0
4
0.178677931
2.432545
2.432545
2.432545
2.432545
1.0
1.0
1.0
1.0
4
0.172296577
2.388712
2.388712
2.388712
2.388712
1.0
1.0
1.0
1.0
4
0.164933475
2.337114
2.337114
2.337114
2.337114
1.0
1.0
1.0
1.0
4
0.156588627

2.277223
2.277223
2.277223
2.277223
1.0
1.0
1.0
1.0
4
0.147262031
2.208365
2.208365
2.208365
2.208365
1.0
1.0
1.0
1.0
4
0.136953689
2.12967
2.12967
2.12967
2.12967
1.0
1.0
1.0
1.0
4
0.1256636
2.04
2.04
2.04
2.04
1.0
1.0
1.0
1.0
4
0.113391764
1.937832
1.937832
1.937832
1.937832
1.0
1.0

1.0
1.0
4
0.100138181
1.821064
1.821064
1.821064
1.821064
1.0
1.0
1.0
1.0
4
0.085902852
1.68666
1.68666
1.68666
1.68666
1.0
1.0
1.0
1.0
4
0.070685775
1.53
1.53
1.53
1.53
1.0
1.0
1.0
1.0
4
0.054486952
1.343296
1.343296
1.343296
1.343296
1.0
1.0
1.0
1.0
4
0.037306381
1.111519
1.111519

1.111519
1.111519
1.0
1.0
1.0
1.0
4
0.019144064
0.796237
0.796237
0.796237
0.796237
1.0
1.0
1.0
1.0

| | | |
|---|---|---|
| 4 | ← | Number of roughness elements at the final height level. |
| 0 | | Blockage fraction, $1-\beta$, at the final height level. |
| 0 | | Diameter for roughness element #1 (mm) |
| 0 | | Diameter for roughness element #2 |
| 0 | | Diameter for roughness element #3 |
| 0 | | Diameter for roughness element #4 |
| 1.0 | | Eccentricity factor for roughness element #1 |
| 1.0 | | Eccentricity factor for roughness element #2 |
| 1.0 | | Eccentricity factor for roughness element #3 |
| 1.0 | | Eccentricity factor for roughness element #4 |